

ION-CYCLOTRON INSTABILITY IN CURRENT-CARRYING LORENTZIAN (KAPPA) AND MAXWELLIAN PLASMAS WITH ANISOTROPIC TEMPERATURES: A COMPARATIVE STUDY

B. Basu and N.J. Grossbard

26 September 2011

Interim Report

APPROVED FOR PUBLIC RELEASE; DISTRIBUTION IS UNLIMITED.



**AIR FORCE RESEARCH LABORATORY
Space Vehicles Directorate
3550 Aberdeen Ave SE
AIR FORCE MATERIEL COMMAND
KIRTLAND AIR FORCE BASE, NM 87117-5776**

DTIC COPY

NOTICE AND SIGNATURE PAGE

Using Government drawings, specifications, or other data included in this document for any purpose other than Government procurement does not in any way obligate the U.S. Government. The fact that the Government formulated or supplied the drawings, specifications, or other data does not license the holder or any other person or corporation; or convey any rights or permission to manufacture, use, or sell any patented invention that may relate to them.

This report was cleared for public release by the Air Force Research Laboratory [insert TD site] Public Affairs Office and is available to the general public, including foreign nationals. Copies may be obtained from the Defense Technical Information Center (DTIC) (<http://www.dtic.mil>).

AFRL-RV-PS-TR-2011-0164 HAS BEEN REVIEWED AND IS APPROVED FOR PUBLICATION IN ACCORDANCE WITH ASSIGNED DISTRIBUTION STATEMENT.

// Signed //
Daniel M. Ober, RVBXP

// Signed //
Joel B. Mozer, Division Chief, RVB

This report is published in the interest of scientific and technical information exchange, and its publication does not constitute the Government's approval or disapproval of its ideas or findings.

REPORT DOCUMENTATION PAGE

Form Approved
OMB No. 0704-0188

Public reporting burden for this collection of information is estimated to average 1 hour per response, including the time for reviewing instructions, searching existing data sources, gathering and maintaining the data needed, and completing and reviewing this collection of information. Send comments regarding this burden estimate or any other aspect of this collection of information, including suggestions for reducing this burden to Department of Defense, Washington Headquarters Services, Directorate for Information Operations and Reports (0704-0188), 1215 Jefferson Davis Highway, Suite 1204, Arlington, VA 22202-4302. Respondents should be aware that notwithstanding any other provision of law, no person shall be subject to any penalty for failing to comply with a collection of information if it does not display a currently valid OMB control number. **PLEASE DO NOT RETURN YOUR FORM TO THE ABOVE ADDRESS.**

1. REPORT DATE (DD-MM-YYYY) 26-09-2011			2. REPORT TYPE Interim Report		3. DATES COVERED (From - To) 1 Oct 2007 – 9 Sep 2011	
4. TITLE AND SUBTITLE Ion-Cyclotron Instability in Current-Carrying Lorentzian (Kappa) and Maxwellian Plasmas with Anisotropic Temperatures: A Comparative Study					5a. CONTRACT NUMBER	
					5b. GRANT NUMBER	
					5c. PROGRAM ELEMENT NUMBER 61102F	
6. AUTHOR(S) B. Basu and N.J. Grossbard*					5d. PROJECT NUMBER 2301	
					5e. TASK NUMBER	
					5f. WORK UNIT NUMBER 837103	
7. PERFORMING ORGANIZATION NAME(S) AND ADDRESS(ES) Air Force Research Laboratory Space Vehicles Directorate 3550 Aberdeen Ave SE Kirtland AFB, NM 87117-5776 *Boston College Institute for Scientific Research 140 Commonwealth Avenue Chestnut Hill, MA 02467					8. PERFORMING ORGANIZATION REPORT NUMBER AFRL-RV-PS-TR-2011-0164	
					9. SPONSORING / MONITORING AGENCY NAME(S) AND ADDRESS(ES)	
					10. SPONSOR/MONITOR'S ACRONYM(S) AFRL/RVBXP	
					11. SPONSOR/MONITOR'S REPORT NUMBER(S)	
12. DISTRIBUTION / AVAILABILITY STATEMENT Approved for public release; distribution is unlimited. (377ABW-2011-0705, dtd 12 May 2011)						
13. SUPPLEMENTARY NOTES Post print from Physics of Plasmas 18 , 2011, pp. 092106-1 – 092106-12; Government Purpose Rights.						
14. ABSTRACT Current-driven electrostatic ion-cyclotron instability has so far been studied for Maxwellian plasma with isotropic and anisotropic temperatures. Since satellite-measured particle velocity distributions in space are often better modeled by the generalized Lorentzian (kappa) distributions and since temperature anisotropy is quite common in space plasmas, theoretical analysis of the current-driven, electrostatic ion-cyclotron instability is carried out in this paper for electron-proton plasma with anisotropic temperatures, where the particle parallel velocity distributions are modeled by kappa distributions and the perpendicular velocity distributions are modeled by Maxwellian distributions. Stability properties of the excited ion cyclotron modes and, in particular, their dependence on electron to ion temperature ratio and ion temperature anisotropy are presented in more detail. For comparison, the corresponding results for bi-Maxwellian plasma are also presented. Although the stability properties of the ion cyclotron modes in the two types of plasmas are qualitatively similar, significant quantitative differences can arise depending on the values of j_e and j_i . The comparative study is based on the numerical solutions of the respective linear dispersion relations. Quasilinear estimates of the resonant ion heating rates due to ion-cyclotron turbulence in the two types of plasma are also presented for comparison.						
15. SUBJECT TERMS Current-driven, electrostatic, ion-cyclotron, instability, Maxwellian, turbulence, anisotropic, Kappa						
16. SECURITY CLASSIFICATION OF:			17. LIMITATION OF ABSTRACT Unlimited	18. NUMBER OF PAGES 16	19a. NAME OF RESPONSIBLE PERSON Daniel Ober	
a. REPORT Unclassified	b. ABSTRACT Unclassified	c. THIS PAGE Unclassified			19b. TELEPHONE NUMBER (include area code)	

Ion-cyclotron instability in current-carrying Lorentzian (κ) and Maxwellian plasmas with anisotropic temperatures: A comparative study

B. Basu^{1,a)} and N. J. Grossbard²

¹*Air Force Research Laboratory, Hanscom Air Force Base, Massachusetts 01731, USA*

²*Boston College, Chestnut Hill, Massachusetts 02467, USA*

(Received 29 April 2011; accepted 12 August 2011; published online 9 September 2011)

Current-driven electrostatic ion-cyclotron instability has so far been studied for Maxwellian plasma with isotropic and anisotropic temperatures. Since satellite-measured particle velocity distributions in space are often better modeled by the generalized Lorentzian (κ) distributions and since temperature anisotropy is quite common in space plasmas, theoretical analysis of the current-driven, electrostatic ion-cyclotron instability is carried out in this paper for electron-proton plasma with anisotropic temperatures, where the particle parallel velocity distributions are modeled by κ distributions and the perpendicular velocity distributions are modeled by Maxwellian distributions. Stability properties of the excited ion cyclotron modes and, in particular, their dependence on electron to ion temperature ratio and ion temperature anisotropy are presented in more detail. For comparison, the corresponding results for bi-Maxwellian plasma are also presented. Although the stability properties of the ion cyclotron modes in the two types of plasmas are qualitatively similar, significant quantitative differences can arise depending on the values of κ_e and κ_i . The comparative study is based on the numerical solutions of the respective linear dispersion relations. Quasilinear estimates of the resonant ion heating rates due to ion-cyclotron turbulence in the two types of plasma are also presented for comparison. © 2011 American Institute of Physics. [doi:10.1063/1.3632974]

I. INTRODUCTION

The satellite-measured particle velocity distributions in the solar wind and in many space plasmas often exhibit non-Maxwellian suprathermal tails that decrease as a power-law of the velocity.¹ Such deviations from the Maxwellian distributions are expected in plasmas with sufficiently low degree of collisionality. The distribution function that can better model such particle velocity distributions is the so-called generalized Lorentzian or kappa (κ) distribution.² The kappa distribution with a finite value of the spectral index κ has a power-law tail at velocities larger than the thermal velocity and, consequently, has a substantially larger number of suprathermal particles in comparison with the Maxwellian distribution. It approaches the Maxwellian distribution in the limit as $\kappa \rightarrow \infty$. Typical values of κ for space plasmas are in the range 2–6. In the last several years, many authors studied electrostatic and electromagnetic waves in spatially homogeneous and weakly inhomogeneous magnetoplasmas using different types of kappa distributions for the equilibrium state.^{1,3–17} The presence of substantially larger number of suprathermal particles in comparison with the Maxwellian was shown to have important distinguishing effects on the spectral properties of the excited waves and on the wave-particle interactions, in particular. In this paper, we present for the first time the stability properties of the electrostatic ion cyclotron modes in current-carrying Lorentzian (κ) plasma with anisotropic electron and ion temperatures and

compare them with those in Maxwellian plasma. The comparative study is based on the numerical solutions of the linear dispersion relations for the two types of plasma. Numerical analysis allows the investigation of parameter regimes that are not accessible to tractable analytical treatments and thus allows a more comprehensive quantitative comparison. Quasilinear estimates of the resonant ion heating rates due to ion cyclotron turbulence in the two types of plasma are also presented for comparison.

Electrostatic ion-cyclotron instability, which considers waves propagating at large angles to the ambient magnetic field with frequency near the ion cyclotron frequency, can arise from various free energy sources such as field-aligned currents,^{18–23} electron beams,²⁴ ion beams^{25,26} or combined effects of ion beams, and counterstreaming electrons.²⁷ We concentrate here on the field-aligned current, which is a common feature in many space and laboratory plasmas, as the free energy source for the ion-cyclotron instability.

Current-driven electrostatic ion-cyclotron instability plays an important role in the generation of ion cyclotron turbulence and in the concomitant anomalous ion heating observed in space and laboratory plasmas. The previous theoretical and numerical studies of the instability assumed that the electron and the ion distributions in velocity space are Maxwellians. Drummond and Rosenbluth¹⁸ first developed the theory of this instability for Maxwellian plasma with isotropic electron and ion temperatures and showed that, for $T_e \approx T_i$, the critical value of the electron drift relative to the stationary ions (i.e., the critical current) for the onset of the instability is much smaller than that for the onset of the electrostatic ion-acoustic instability, which considers waves

^{a)}Present address: Institute for Scientific Research, Boston College, Chestnut Hill, Massachusetts 02467, USA.

propagating parallel to the magnetic field. Kindel and Kennel¹⁹ extended the theoretical analysis of Drummond and Rosenbluth¹⁸ and showed that the ion cyclotron waves are unstable to smaller currents for a broad range of T_e/T_i . The effects of temperature anisotropies, which are also important features of collisionless plasmas, on the excitation of the current-driven electrostatic ion-cyclotron instability in Maxwellian plasma were first investigated by Lee,²¹ who followed the theoretical analysis of Kindel and Kennel.¹⁹ Later, Okuda and Ashour-Abdalla^{22,23} investigated the effects of temperature anisotropies over a wider range of parameters by numerically solving the dispersion relation. For a review of these previous studies, see Ref. 28.

In Sec. II, we present the mathematical model and the linear dispersion relations for the current-driven ion cyclotron modes in Maxwellian and Lorentzian (kappa) plasmas. In Sec. III, we present the approximate analysis of the dispersion relations in order to gain some preliminary understanding of the differences in the stability properties of the ion cyclotron modes in the two types of plasma. In Sec. IV, we present the numerical solutions of the dispersion relations. In Sec. V, we calculate the resonant ion heating rates due to ion-cyclotron turbulence in the two types of plasma, within the framework of the quasilinear theory, and discuss their differences. The paper is concluded with a summary in Sec. VI.

II. LINEAR DISPERSION RELATION FOR CURRENT-DRIVEN ION CYCLOTRON MODES

The starting point of our study is the linear dispersion relation for obliquely propagating electrostatic ion cyclotron modes in current-carrying plasma with anisotropic electron and ion temperatures. For this, we consider spatially homogeneous, nonrelativistic, collisionless plasma in which electrons are drifting along the uniform ambient magnetic field \mathbf{B}_0 with velocity \mathbf{V}_0 relative to the stationary ions. Considering normal modes of the form $\exp[i(\mathbf{k} \cdot \mathbf{r} - \omega t)]$ with frequency ω and propagation vector \mathbf{k} , we assume $|(\omega - k_{\parallel} V_0)/\Omega_e| \ll 1$, $|k_{\parallel} V_{e\parallel}/\Omega_e| \ll 1$ and $k_{\perp} V_{e\perp}/\Omega_e \ll 1$, where $\Omega_e = eB_0/(m_e c)$ is the electron cyclotron frequency, $V_{e\parallel}$ and $V_{e\perp}$ are the electron thermal speeds defined as $V_{e\parallel(\perp)}^2 = T_{e\parallel(\perp)}/m_e$, $k_{\parallel} = (\mathbf{k} \cdot \mathbf{B}_0)/B_0$, and k_{\perp} is the perpendicular (to \mathbf{B}_0) component of \mathbf{k} . We further assume that $\omega_{pe}/\Omega_e \ll 1$, where ω_{pe} is the electron plasma frequency. These assumptions imply that the electrons are strongly magnetized particles so that their dynamic response to the electric field perturbation is practically one-dimensional (parallel to \mathbf{B}_0). For the ion response, however, we retain both the parallel and the perpendicular dynamics. Then, according to the linearized Vlasov theory, the dispersion relation for obliquely propagating electrostatic waves is given by²⁹

$$1 + \frac{4\pi e^2}{m_e k^2} \int \frac{d\mathbf{v}}{\omega - k_{\parallel} v_{\parallel}} k_{\parallel} \frac{\partial}{\partial v_{\parallel}} F_e(v_{\perp}^2, v_{\parallel}) + \frac{4\pi e^2}{m_i k^2} \times \sum_{n=-\infty}^{+\infty} \int d\mathbf{v} \frac{J_n^2(\mu)}{\omega - k_{\parallel} v_{\parallel} - n\Omega_i} \left(k_{\parallel} \frac{\partial}{\partial v_{\parallel}} + \frac{n\Omega_i}{v_{\perp}} \frac{\partial}{\partial v_{\perp}} \right) \times F_i(v_{\perp}^2, v_{\parallel}) = 0, \quad (1)$$

for $\text{Im } \omega > 0$. Here $F_{\alpha}(v_{\perp}^2, v_{\parallel})$ is the unperturbed (equilibrium) distribution function for the charged particle species $\alpha = e, i$, $\Omega_i = eB_0/(m_i c)$, $J_n(\mu)$ is the Bessel function of order n , $\mu = k_{\perp} v_{\perp}/\Omega_i$, and $k^2 = k_{\parallel}^2 + k_{\perp}^2$. For analytic continuation to $\text{Im } \omega \leq 0$, the Landau contour has to be used for carrying out the v_{\parallel} integration. The two types of equilibrium distribution function, considered here for the derivation of the linear dispersion relation, are the following.

A. Bi-Maxwellian

$$F_{\alpha}(v_{\perp}^2, v_{\parallel}) = \frac{n_0}{\pi^{3/2} \theta_{\alpha\parallel} \theta_{\alpha\perp}^2} \exp\left(-\frac{v_{\perp}^2}{\theta_{\alpha\perp}^2}\right) \exp\left(-\frac{u_{\alpha\parallel}^2}{\theta_{\alpha\parallel}^2}\right), \quad (2)$$

where $u_{\alpha\parallel} \equiv v_{\parallel} - V_{\alpha 0}$ with $V_{\alpha 0} = V_0$ for the electrons and $V_{\alpha 0} = 0$ for the ions, $\theta_{\alpha\parallel(\perp)}^2$ is related to the particle temperature $T_{\alpha\parallel(\perp)}$ by $\theta_{\alpha\parallel(\perp)}^2 = 2T_{\alpha\parallel(\perp)}/m_{\alpha} \equiv 2V_{\alpha\parallel(\perp)}^2$, and F_{α} is normalized to the particle density n_0 (same for both electrons and ions). The definitions of $T_{\alpha\parallel}$ and $T_{\alpha\perp}$ are

$$n_0 T_{\alpha\parallel} = 2\pi m_{\alpha} \int dv_{\perp} dv_{\parallel} v_{\perp} u_{\alpha\parallel}^2 F_{\alpha}(v_{\perp}^2, v_{\parallel}), \quad (3)$$

$$n_0 T_{\alpha\perp} = \pi m_{\alpha} \int dv_{\perp} dv_{\parallel} v_{\perp}^3 F_{\alpha}(v_{\perp}^2, v_{\parallel}). \quad (4)$$

Substituting $F_{\alpha}(v_{\perp}^2, v_{\parallel})$, given by Eq. (2), into Eq. (1) and performing the velocity space integrations, we obtain the well-known dispersion relation

$$D(\mathbf{k}, \omega) \equiv 1 - \frac{\omega_{pe}^2}{k^2 \theta_{e\parallel}^2} Z'_M(\zeta_e) - \frac{\omega_{pi}^2}{k^2 \theta_{i\parallel}^2} \sum_{n=-\infty}^{+\infty} \Lambda_n(b_i) \times \left[Z'_M(\zeta_{ni}) - \frac{2n\Omega_i}{k_{\parallel} \theta_{i\parallel}} \frac{\theta_{i\parallel}^2}{\theta_{i\perp}^2} Z_M(\zeta_{ni}) \right] = 0. \quad (5)$$

Here, $\omega_{p\alpha}^2 = 4\pi e^2 n_0/m_{\alpha}$, $\Lambda_n(b_i) = I_n(b_i) \exp(-b_i)$, I_n is the modified Bessel function of the first kind, $b_i = k_{\perp}^2 \theta_{i\perp}^2 / (2\Omega_i^2)$, $\zeta_e = (\omega - k_{\parallel} V_0)/(k_{\parallel} \theta_{e\parallel})$, and $\zeta_{ni} = (\omega - n\Omega_i)/(k_{\parallel} \theta_{i\parallel})$, where $k_{\parallel} > 0$ is assumed. $Z_M(\zeta)$ is the well-known plasma dispersion function³⁰ associated with the Maxwellian v_{\parallel} -distribution and it is defined as

$$Z_M(\zeta) = \frac{1}{\sqrt{\pi}} \int_{-\infty}^{+\infty} ds \frac{\exp(-s^2)}{s - \zeta}, \quad (6)$$

for $\text{Im } \zeta > 0$ and as the analytic continuation of this for $\text{Im } \zeta \leq 0$. The prime notation on $Z_M(\zeta)$ denotes its derivative with respect to the argument.

B. Kappa-Maxwellian

$$F_{\alpha}(v_{\perp}^2, v_{\parallel}) = \frac{n_0 f(\kappa_{\alpha})}{\pi^{3/2} \theta_{\alpha\parallel} \theta_{\alpha\perp}^2} \left(1 + \frac{u_{\alpha\parallel}^2}{\kappa_{\alpha} \theta_{\alpha\parallel}^2} \right)^{-(\kappa_{\alpha}+1)} \exp\left(-\frac{v_{\perp}^2}{\theta_{\alpha\perp}^2}\right), \quad (7)$$

where $f(\kappa_{\alpha}) = \Gamma(\kappa_{\alpha} + 1)/[\kappa_{\alpha}^{1/2} \Gamma(\kappa_{\alpha} + 1/2)]$, $\Gamma(x)$ being the gamma function. As before, $u_{\alpha\parallel} \equiv v_{\parallel} - V_{\alpha 0}$ with $V_{\alpha 0} = V_0$

for the electrons, $V_{\alpha 0} = 0$ for the ions, and F_α is normalized to the particle density n_0 (same for both electrons and ions), while $\theta_{\alpha\parallel}^2$ and $\theta_{\alpha\perp}^2$ are related to the particle “temperatures” $T_{\alpha\parallel}$ and $T_{\alpha\perp}$, as defined by Eqs. (3) and (4), according to $\theta_{\alpha\parallel}^2 = [(2\kappa_\alpha - 1)/\kappa_\alpha](T_{\alpha\parallel}/m_\alpha) \equiv [(2\kappa_\alpha - 1)/\kappa_\alpha]V_{\alpha\parallel}^2$ and $\theta_{\alpha\perp}^2 = 2T_{\alpha\perp}/m_\alpha \equiv 2V_{\alpha\perp}^2$, provided $\kappa_\alpha > 1/2$. As $\kappa_\alpha \rightarrow \infty$, F_α [given by Eq. (7)] asymptotically approaches the bi-Maxwellian [given by Eq. (2)]. In Eq. (7), the particle distribution in v_{\parallel} —space is modeled by the kappa distribution function, while the distribution in v_{\perp} —space is modeled by the Maxwellian distribution. The physical arguments for not considering a kappa distribution in v_{\perp} —space are the following. First, in the presence of an ambient magnetic field, the mechanism that produces the kappa type distribution in velocity space is most likely to be more effective in v_{\parallel} —space. Second, the most important physical aspect of the kappa distribution, which distinguishes it from the Maxwellian distribution, is the resonant wave-particle interaction (Landau and cyclotron resonances) between the excited waves and the enhanced population of suprathermal charged particles that are moving along the ambient magnetic field. It may be mentioned, however, that a kappa distribution in v_{\perp} —space does not pose a serious mathematical difficulty. With it, the velocity integral in the ion term involving J_n^2 and $(\partial F_i/\partial v_{\perp})$ cannot be expressed in terms of any known mathematical function; but, it can be numerically evaluated quite easily. The integral approaches its Maxwellian counterpart, $\Lambda_n(b_i)$, in the limit as $\kappa_i \rightarrow \infty$, and its numerical values for finite values of κ_i are not too different from those of $\Lambda_n(b_i)$.

Substituting $F_\alpha(v_{\perp}, v_{\parallel})$, given by Eq. (7), into Eq. (1) and performing the velocity space integrations, the dispersion relation is obtained as

$$D(\mathbf{k}, \omega) \equiv 1 - \frac{\omega_{pe}^2}{k^2 \theta_{e\parallel}^2} Z'_{\kappa_e}(\zeta_e) - \frac{\omega_{pi}^2}{k^2 \theta_{i\parallel}^2} \sum_{n=-\infty}^{+\infty} \Lambda_n(b_i) \times \left[Z'_{\kappa_i}(\zeta_{ni}) - \frac{2n\Omega_i}{k_{\parallel}\theta_{i\parallel}} \frac{\theta_{i\parallel}^2}{\theta_{i\perp}^2} Z_{\kappa_i}(\zeta_{ni}) \right] = 0, \quad (8)$$

where $\Lambda_n(b_i) = I_n(b_i) \exp(-b_i)$, I_n is the modified Bessel function of the first kind, $b_i = k_{\perp}^2 \theta_{i\perp}^2 / (2\Omega_i^2)$, $\zeta_e = (\omega - k_{\parallel}V_0)/(k_{\parallel}\theta_{e\parallel})$, and $\zeta_{ni} = (\omega - n\Omega_i)/(k_{\parallel}\theta_{i\parallel})$ with $k_{\parallel} > 0$. The dispersion relation for kappa-Maxwellian plasma is formally equivalent to that for the bi-Maxwellian plasma, except that $\theta_{\alpha\parallel}^2 = (T_{\alpha\parallel}/m_\alpha)[(2\kappa_\alpha - 1)/\kappa_\alpha]$ and $Z_{\kappa_\alpha}(\zeta)$ is the modified plasma dispersion function associated with the kappa distribution function in v_{\parallel} —space. The modified plasma dispersion function is defined by^{16,17}

$$Z_{\kappa_\alpha}(\zeta) = \frac{f(\kappa_\alpha)}{\sqrt{\pi}} \int_{-\infty}^{+\infty} \frac{ds}{(s - \zeta)(1 + s^2/\kappa_\alpha)^{\kappa_\alpha+1}}, \quad (9)$$

for $\text{Im } \zeta > 0$ and by the analytic continuation of this for $\text{Im } \zeta \leq 0$. The prime notation on $Z_{\kappa_\alpha}(\zeta)$ denotes its derivative with respect to the argument. Aside from the multiplication factor, this function is analogous to the plasma dispersion function that was first introduced and discussed by Summers and Thorne³ and was later further analyzed by Mace and Hellberg³¹ and Summers *et al.*³²

III. APPROXIMATE STABILITY ANALYSIS

Here, we present the approximate analytical solutions of the dispersion relations in order to gain some preliminary understanding of the ion-cyclotron instability in the two types of plasmas. Considering $\omega = \text{Re } \omega + i \text{Im } \omega$ and making a Taylor series expansion of $D(\mathbf{k}, \omega)$ around $\omega = \text{Re } \omega$ while assuming $\text{Im } \omega \ll \text{Re } \omega$ and $\text{Im } D \ll \text{Re } D$, we find to lowest order,

$$\text{Re } D(\mathbf{k}, \omega = \text{Re } \omega) = 0, \quad (10)$$

$$\text{Im } \omega = - \frac{\text{Im } D(\mathbf{k}, \omega = \text{Re } \omega)}{[\partial \text{Re } D(\mathbf{k}, \omega)/\partial \omega]_{\omega = \text{Re } \omega}}. \quad (11)$$

These two equations determine $\text{Re } \omega$ and $\text{Im } \omega$. Generally speaking, unstable solutions are found when $\text{Re } \omega/k_{\parallel} < V_0$ (i.e., $\text{Re } \zeta_e < 0$) so that $(\partial F_e/\partial v_{\parallel})|_{v_{\parallel} = \text{Re } \omega/k_{\parallel}} > 0$ (Landau growth) and, simultaneously, when (a) $\text{Re } \zeta_{mi} > 1$ for cyclotron modes with $\text{Re } \omega \approx m\Omega_i$; and (b) $\text{Re } \zeta_{ni} \gg 1$ for all $n \neq m$, such that the Landau growth rate due to the drifting (current-carrying) electrons exceeds the total ion damping (both Landau and cyclotron damping) rate. For the approximate stability analysis, we follow the commonly used analytical approach of Drummond and Rosenbluth,¹⁸ i.e., we consider $|\zeta_e| \ll 1$ and $|\zeta_{ni}| \gg 1$ for all n and retain the leading terms in the power series expansion of the electron plasma dispersion function and the asymptotic expansion of the ion plasma dispersion function. The power series and the asymptotic expansions of $Z_M(\zeta)$ are³⁰

$$Z_M(\zeta) = i\sqrt{\pi} \exp(-\zeta^2) - 2\zeta + 4\zeta^3/3 - \dots, \quad |\zeta| \ll 1, \quad (12)$$

$$Z_M(\zeta) \cong i\sqrt{\pi} \exp(-\zeta^2) - \frac{1}{\zeta} - \frac{1}{2\zeta^3} - \dots, \quad |\zeta| \gg 1, \quad (13)$$

while the power series and the asymptotic expansions of $Z_{\kappa_\alpha}(\zeta)$ for integer values of κ_α are^{3,17,18}

$$Z_{\kappa_\alpha}(\zeta) = i\sqrt{\pi} \frac{f(\kappa_\alpha)}{(1 + \zeta^2/\kappa_\alpha)^{\kappa_\alpha+1}} - \frac{2\kappa_\alpha + 1}{\kappa_\alpha} \zeta \left(1 - \frac{2\kappa_\alpha + 3}{3\kappa_\alpha} \zeta^2 + \dots \right), \quad |\zeta| \ll 1, \quad (14)$$

$$Z_{\kappa_\alpha}(\zeta) = i\sqrt{\pi} \frac{f(\kappa_\alpha)}{(1 + \zeta^2/\kappa_\alpha)^{\kappa_\alpha+1}} - \frac{1}{\zeta} - \frac{\kappa_\alpha}{2\kappa_\alpha - 1} \frac{1}{\zeta^3} - \dots, \quad |\zeta| \gg 1. \quad (15)$$

For noninteger (including half-integer) values of κ_α , the asymptotic expansion has small correction terms,^{31,32} which may be neglected.

A. Bi-Maxwellian plasma

Restricting ourselves to the fundamental ion cyclotron mode, i.e., $\text{Re } \omega \approx \Omega_i$, we retain only the $n = 1$ term in the ion sum. Using the leading terms of Eqs. (12) and (13) in Eq. (5), we find

$$\operatorname{Re} D(\mathbf{k}, \omega = \operatorname{Re} \omega) \cong 1 + \frac{2\omega_{pe}^2}{k^2\theta_{e\parallel}^2} - \frac{2\omega_{pi}^2}{k^2\theta_{i\parallel}^2} \frac{\theta_{i\parallel}^2}{\theta_{i\perp}^2} \frac{\Omega_i}{\operatorname{Re} \omega - \Omega_i} \Lambda_1(b_i), \quad (16)$$

$$\begin{aligned} \operatorname{Im} D(\mathbf{k}, \omega = \operatorname{Re} \omega) &\cong 2i\sqrt{\pi} \frac{\omega_{pe}^2}{k^2\theta_{e\parallel}^2} \frac{\operatorname{Re} \omega - k_{\parallel} V_0}{k_{\parallel}\theta_{e\parallel}} \\ &+ 2i\sqrt{\pi} \frac{\omega_{pi}^2}{k^2\theta_{i\parallel}^2} \frac{\operatorname{Re} \omega - (1 - \theta_{i\parallel}^2/\theta_{i\perp}^2)\Omega_i}{k_{\parallel}\theta_{i\parallel}} \\ &\times \Lambda_1(b_i) \exp(-\zeta_{1i}^2). \end{aligned} \quad (17)$$

Then, referring to Eqs. (10) and (11), we obtain

$$\frac{\operatorname{Re} \omega}{\Omega_i} = 1 + \frac{T_{e\parallel}}{T_{i\parallel}} \frac{T_{i\parallel}}{T_{i\perp}} \frac{\Lambda_1(b_i)}{1 + k^2\lambda_{De}^2}, \quad (18)$$

$$\begin{aligned} \frac{\operatorname{Im} \omega}{\Omega_i} &= \sqrt{\frac{\pi}{2}} \frac{T_{e\parallel}}{T_{i\parallel}} \frac{T_{i\parallel}}{T_{i\perp}} \frac{\Lambda_1(b_i)}{(1 + k^2\lambda_{De}^2)^2} \left[\frac{k_{\parallel} V_0 - \operatorname{Re} \omega}{k_{\parallel} V_{e\parallel}} \right. \\ &\left. - \frac{T_{e\parallel}}{T_{i\parallel}} \frac{\operatorname{Re} \omega - (1 - T_{i\parallel}/T_{i\perp})\Omega_i}{k_{\parallel} V_{i\parallel}} \Lambda_1(b_i) \exp(-\eta_i^2) \right], \end{aligned} \quad (19)$$

where $\eta_i \equiv (\operatorname{Re} \omega - \Omega_i)/(\sqrt{2}k_{\parallel}V_{i\parallel})$. We have related $\theta_{\alpha\parallel(\perp)}^2$ to $T_{\alpha\parallel(\perp)}$ and introduced the Debye length, λ_{De} , defined by $\lambda_{De}^2 = T_{e\parallel}/(m_e\omega_{pe}^2)$. The onset condition for instability ($\operatorname{Im} \omega > 0$) is

$$\frac{V_0}{V_{e\parallel}} > \frac{\operatorname{Re} \omega}{k_{\parallel} V_{e\parallel}} + \frac{T_{e\parallel}}{T_{i\parallel}} \frac{\operatorname{Re} \omega - (1 - T_{i\parallel}/T_{i\perp})\Omega_i}{k_{\parallel} V_{i\parallel}} \Lambda_1(b_i) \exp(-\eta_i^2). \quad (20)$$

$$\begin{aligned} \frac{\operatorname{Im} \omega}{\Omega_i} &= \sqrt{\frac{\pi}{2}} \frac{(2\kappa_e - 1)^2 T_{e\parallel} T_{i\parallel}}{(2\kappa_e + 1) T_{i\parallel} T_{i\perp}} \frac{\Lambda_1(b_i)}{\{1 + [(2\kappa_e - 1)/(2\kappa_e + 1)]k^2\lambda_{De}^2\}^2} \\ &\times \left\{ \frac{k_{\parallel} V_0 - \operatorname{Re} \omega \kappa_e + 1}{k_{\parallel} V_{e\parallel}} \frac{1}{\kappa_e} \left(\frac{2\kappa_e}{2\kappa_e - 1} \right)^{3/2} f(\kappa_e) - \frac{T_{e\parallel}}{T_{i\parallel}} \frac{\Lambda_1(b_i)}{k_{\parallel} V_{i\parallel}} \left(\frac{2\kappa_i}{2\kappa_i - 1} \right)^{3/2} f(\kappa_i) \right. \\ &\left. \times \left(1 + \frac{\eta_i^2}{\kappa_i - 1/2} \right)^{-(\kappa_i+1)} \left[\left(1 + \frac{\eta_i^2}{\kappa_i - 1/2} \right)^{-1} \frac{\kappa_i + 1}{\kappa_i} (\operatorname{Re} \omega - \Omega_i) + \frac{2\kappa_i - 1}{2\kappa_i} \frac{T_{i\parallel}}{T_{i\perp}} \Omega_i \right] \right\}, \end{aligned} \quad (24)$$

where $\eta_i = (\operatorname{Re} \omega - \Omega_i)/(\sqrt{2}k_{\parallel}V_{i\parallel})$. We have related $\theta_{\alpha\parallel(\perp)}^2$ to $T_{\alpha\parallel(\perp)}$ and introduced the Debye length λ_{De} . The onset condition for instability ($\operatorname{Im} \omega > 0$) is

$$\begin{aligned} \frac{V_0}{V_{e\parallel}} &> \frac{\operatorname{Re} \omega}{k_{\parallel} V_{e\parallel}} + \frac{T_{e\parallel}}{T_{i\parallel}} \\ &\times \left(\frac{2\kappa_i}{2\kappa_i - 1} \right)^{3/2} \left(\frac{2\kappa_e - 1}{2\kappa_e} \right)^{3/2} \frac{\kappa_e}{\kappa_e + 1} \frac{f(\kappa_i) \Lambda_1(b_i)}{f(\kappa_e) k_{\parallel} V_{i\parallel}} \\ &\times \left(1 + \frac{\eta_i^2}{\kappa_i - 1/2} \right)^{-(\kappa_i+1)} \left[\left(1 + \frac{\eta_i^2}{\kappa_i - 1/2} \right)^{-1} \right. \\ &\left. \times \frac{\kappa_i + 1}{\kappa_i} (\operatorname{Re} \omega - \Omega_i) + \frac{2\kappa_i - 1}{2\kappa_i} \frac{T_{i\parallel}}{T_{i\perp}} \Omega_i \right]. \end{aligned} \quad (25)$$

These results for anisotropic ion temperatures ($T_{i\parallel} \neq T_{i\perp}$) were previously obtained by Lee²¹ and by Okuda and Ashour-Abdalla.²² They reduce to the earlier results of Drummond and Rosenbluth¹⁸ for isotropic ion temperatures ($T_{i\parallel} = T_{i\perp}$).

B. Kappa-Maxwellian plasma

As before, we restrict ourselves to $\operatorname{Re} \omega \approx \Omega_i$ and use the leading terms of Eqs. (14) and (15) in Eq. (8) to find

$$\begin{aligned} \operatorname{Re} D(\mathbf{k}, \omega = \operatorname{Re} \omega) &= 1 + \frac{\omega_{pe}^2}{k^2\theta_{e\parallel}^2} \frac{2\kappa_e + 1}{\kappa_e} \\ &- \frac{2\omega_{pi}^2}{k^2\theta_{i\parallel}^2} \frac{\theta_{i\parallel}^2}{\theta_{i\perp}^2} \frac{\Omega_i}{\operatorname{Re} \omega - \Omega_i} \Lambda_1(b_i), \end{aligned} \quad (21)$$

$$\begin{aligned} \operatorname{Im} D(\mathbf{k}, \omega = \operatorname{Re} \omega) &= 2i\sqrt{\pi} \frac{\omega_{pe}^2}{k^2\theta_{e\parallel}^2} \frac{\operatorname{Re} \omega - k_{\parallel} V_0 \kappa_e + 1}{k_{\parallel}\theta_{e\parallel}} \frac{1}{\kappa_e} f(\kappa_e) \\ &+ 2i\sqrt{\pi} \frac{\omega_{pi}^2}{k^2\theta_{i\parallel}^2} \frac{\Lambda_1(b_i)}{k_{\parallel}\theta_{i\parallel}} \frac{f(\kappa_i)}{(1 + \zeta_{1i}^2/\kappa_i)^{\kappa_i+1}} \\ &\times \left(\frac{\kappa_i + 1 \operatorname{Re} \omega - \Omega_i}{\kappa_i} \frac{1 + \theta_{i\parallel}^2/\theta_{i\perp}^2}{1 + \zeta_{1i}^2/\kappa_i} \Omega_i \right). \end{aligned} \quad (22)$$

Then, referring to Eqs. (10) and (11), we obtain

$$\begin{aligned} \frac{\operatorname{Re} \omega}{\Omega_i} &= 1 \\ &+ \frac{T_{e\parallel}}{T_{i\parallel}} \frac{T_{i\parallel}}{T_{i\perp}} \frac{2\kappa_e - 1}{2\kappa_e + 1} \frac{\Lambda_1(b_i)}{1 + [(2\kappa_e - 1)/(2\kappa_e + 1)]k^2\lambda_{De}^2}, \end{aligned} \quad (23)$$

The results presented in Eqs. (21)–(25) are new and they reduce to the corresponding results for bi-Maxwellian plasma [Eqs. (16)–(20)] when $\kappa_e, \kappa_i \rightarrow \infty$.

The approximate analytical solutions indicate that the stability properties of the current-driven ion cyclotron modes in both types of plasma (bi-Maxwellian and kappa-Maxwellian) depend on m_e/m_i , ω_{pe}/Ω_e , V_0 , k_{\parallel} , k_{\perp} , electron to ion temperature ratio ($T_{e\parallel}/T_{i\parallel}$), and ion temperature anisotropy ($T_{i\parallel}/T_{i\perp}$). Dependence on ω_{pe}/Ω_e arises through the term $\omega_{pe}^2/(k^2\theta_{e\parallel}^2)$ in the dispersion relations as $\omega_{pe}^2/(k^2\theta_{e\parallel}^2) \propto (k^2\lambda_{De}^2)^{-1} = (m_i/m_e)(\omega_{pe}^2/\Omega_e^2)/(k^2\rho_i^2)$, where $\rho_i (\equiv V_{i\perp}/\Omega_i)$ is the ion gyroradius. The analytical solutions also indicate that $\operatorname{Re} \omega$, $\operatorname{Im} \omega$, and the onset condition for instability in kappa-Maxwellian plasma can be quite

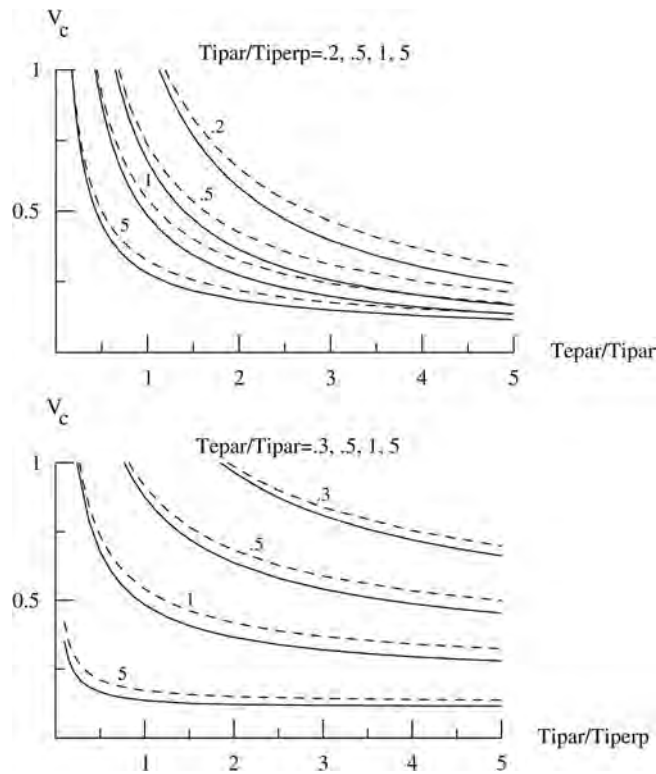


FIG. 1. Threshold (critical) value of electron drift speed, normalized to $V_{e\parallel}$ and denoted by V_C , as a function of $T_{e\parallel}/T_{i\parallel}$ and $T_{i\parallel}/T_{i\perp}$ for $\omega_{pe}/\Omega_e = 1/15$. The solid curves represent results for bi-Maxwellian plasma and the dashed curves represent results for kappa-Maxwellian ($\kappa_e = \kappa_i = 3$) plasma. The curves are labeled by the selected values of $T_{i\parallel}/T_{i\perp}$ and $T_{e\parallel}/T_{i\parallel}$.

different from those in bi-Maxwellian plasma depending on the choice of the values of κ_e and κ_i . Comparison shows that $\text{Re } \omega$ is reduced in kappa-Maxwellian plasma, while both the electron term that drives the instability when $V_0 > \text{Re } \omega/k_{\parallel}$ and the ion cyclotron damping term in $\text{Im } \omega$ are enhanced in kappa-Maxwellian plasma. The enhancement of the electron-drive term in kappa-Maxwellian plasma is due to the reduction of $\text{Re } \omega$ and the multiplying factors involving κ_e . The enhancement of the ion cyclotron damping term in kappa-Maxwellian plasma is predominantly due to its power-law dependence on $\eta_i > 1$ in contrast with its exponential dependence on $\eta_i > 1$ in bi-Maxwellian plasma. For the same reason, the threshold value of V_0 for the onset of the instability in kappa-Maxwellian plasma is enhanced over the corresponding value in bi-Maxwellian plasma.

We shall not pursue the analytical solutions any further as they are valid only for the restricted values of the aforementioned parameters for which the assumed conditions ($|\zeta_e| \ll 1$ and $|\zeta_{ni}| \gg 1$ for all n) can be satisfied. Outside the range of validity, the analytical solutions are not only quantitatively inaccurate; they even give erroneous dependence on k_{\parallel} , for example. For an accurate and comprehensive study of the entire unstable spectrum of the current-driven ion-cyclotron modes, it is, therefore, necessary to solve the dispersion relations numerically. Indeed, numerical analysis shows that the assumed conditions ($|\zeta_e| \ll 1$ and $|\zeta_{ni}| \gg 1$ for all n) are rather difficult to satisfy, particularly when the maximum values of the growth rates occur.

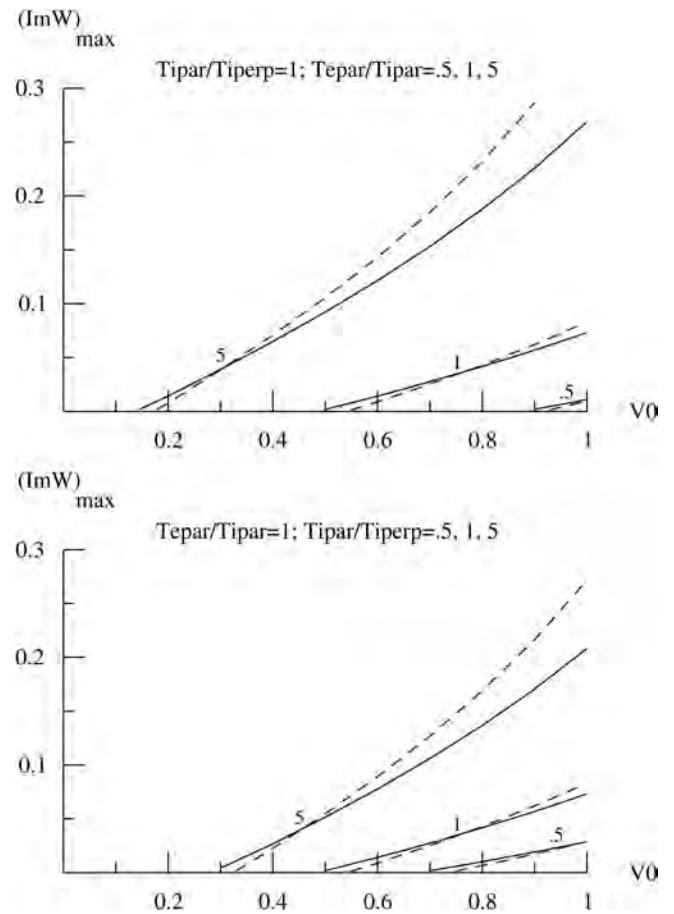


FIG. 2. $\text{Im } \omega$ ($\equiv \text{Im } \omega/\Omega_i$), maximized with respect to k_{\parallel} and k_{\perp} , as a function of V_0 ($\equiv V_0/V_{e\parallel}$) for $\omega_{pe}/\Omega_e = 1/15$ and selected values of $T_{e\parallel}/T_{i\parallel}$ and $T_{i\parallel}/T_{i\perp}$. The solid curves represent results for bi-Maxwellian plasma and the dashed curves represent results for kappa-Maxwellian ($\kappa_e = \kappa_i = 3$) plasma. The curves are labeled by the selected values of $T_{e\parallel}/T_{i\parallel}$ and $T_{i\parallel}/T_{i\perp}$.

IV. NUMERICAL SOLUTIONS OF THE DISPERSION RELATIONS

We have developed a numerical code that evaluates the plasma dispersion functions $Z_M(\zeta)$, $Z_{\kappa_z}(\zeta)$ and solves the dispersion relations to find the complex values of ω ($= \omega_r + i\gamma$) as a function of the aforementioned variable parameters. Here, we consider the electron-proton plasma ($m_e/m_i = 1/1836$) and concentrate on the solutions with $\omega_r \approx \Omega_i$. For kappa-Maxwellian plasma, $\kappa_e = \kappa_i = 3$ is assumed. The numerical results, graphically presented in Figs. 1–9, 13, and 14, are obtained by assuming $\omega_{pe}/\Omega_e = 1/15$, which is consistent with the assumption $\omega_{pe}/\Omega_e \ll 1$ used in the derivation of the dispersion relations. The important effects of ω_{pe}/Ω_e on the stability properties are discussed later in this section by means of Figs. 10–12.

Figure 1 shows the threshold values (critical values) of V_0 (normalized to $V_{e\parallel}$ and denoted by V_C), above which the instability is excited, as a function of $T_{e\parallel}/T_{i\parallel}$ and $T_{i\parallel}/T_{i\perp}$. The threshold values are obtained by minimizing $V_0/V_{e\parallel}$ with respect to both k_{\parallel} and k_{\perp} . In this figure and in all the other figures, the solid curves represent the results for bi-Maxwellian plasma and the dashed curves for kappa-

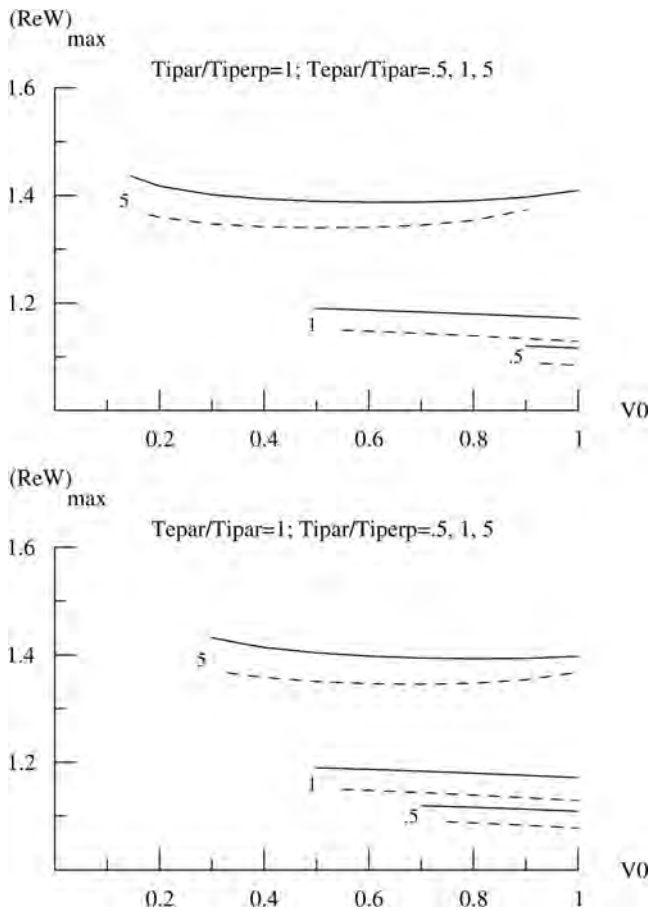


FIG. 3. $\text{Re}W (\equiv \text{Re} \omega / \Omega_i)$, corresponding to $(\text{Im}W)_{\text{max}}$ shown in Fig. 2, as a function of $V0 (\equiv V_0 / V_{e\parallel})$ for $\omega_{pe} / \Omega_e = 1/15$ and selected values of $T_{e\parallel} / T_{i\parallel}$ and $T_{i\parallel} / T_{i\perp}$. The solid curves represent results for bi-Maxwellian plasma and the dashed curves represent results for kappa-Maxwellian ($\kappa_e = \kappa_i = 3$) plasma. The curves are labeled by the selected values of $T_{e\parallel} / T_{i\parallel}$ and $T_{i\parallel} / T_{i\perp}$.

Maxwellian plasma. The top panel of Fig. 1 shows that, for a fixed value of $T_{i\parallel} / T_{i\perp}$, the value of V_C in both types of plasmas decreases sharply as $T_{e\parallel} / T_{i\parallel}$ increases and then settles down to a value which is nearly independent of $T_{e\parallel} / T_{i\parallel}$. It also indicates that, for a fixed value of $T_{e\parallel} / T_{i\parallel}$, the value of V_C decreases as $T_{i\parallel} / T_{i\perp}$ increases. This is shown more explicitly in the bottom panel of Fig. 1. The results for bi-Maxwellian plasma are in agreement with those obtained earlier.^{21–23} The new results in Fig. 1 are that a larger V_C (i.e., larger current) is needed to excite the instability in kappa-Maxwellian plasma for all $T_{i\parallel} / T_{i\perp}$ and for all $T_{e\parallel} / T_{i\parallel}$ above a certain value, which increases with decreasing $T_{i\parallel} / T_{i\perp}$.

Figure 2 shows the maximum values of $\text{Im}W (\equiv \text{Im} \omega / \Omega_i)$ [maximized with respect to k_{\parallel} , k_{\perp} and denoted by $(\text{Im}W)_{\text{max}}$] as a function of $V0 (\equiv V_0 / V_{e\parallel})$ for selected values of $T_{e\parallel} / T_{i\parallel}$ and $T_{i\parallel} / T_{i\perp}$. Figure 3 shows the corresponding values of $\text{Re}W (\equiv \text{Re} \omega / \Omega_i)$, denoted by $(\text{Re}W)_{\text{max}}$, as a function of $V0 (\equiv V_0 / V_{e\parallel})$ for the same values of $T_{e\parallel} / T_{i\parallel}$ and $T_{i\parallel} / T_{i\perp}$. As expected, for all values of $T_{e\parallel} / T_{i\parallel}$, $T_{i\parallel} / T_{i\perp}$ and for both types of plasma, $(\text{Im}W)_{\text{max}}$ decreases as $V0$ decreases toward the threshold values. However, the new and interesting result is that, for all values of $T_{e\parallel} / T_{i\parallel}$ and $T_{i\parallel} / T_{i\perp}$, $(\text{Im}W)_{\text{max}}$ in kappa-Maxwellian plasma

is larger than that in bi-Maxwellian plasma when $V0$ is much larger than the threshold value; decreases more rapidly as $V0$ decreases; and then becomes smaller as $V0$ approaches the threshold value V_C . This is consistent with the results presented in Fig. 1, namely, V_C is larger for kappa-Maxwellian plasma. Figure 3 shows that $(\text{Re}W)_{\text{max}}$ is smaller in kappa-Maxwellian plasma than in bi-Maxwellian plasma for all values of $V0 > V_C$, $T_{e\parallel} / T_{i\parallel}$, and $T_{i\parallel} / T_{i\perp}$. It should be pointed out that the approximate analytical solutions in Sec. III do not show the dependence, albeit weak, of the real frequency on $V0$. As Fig. 2 indicates the maximum linear growth rate of the instability can be somewhat large when $T_{e\parallel} / T_{i\parallel}$, $T_{i\parallel} / T_{i\perp}$ are large (> 1) and simultaneously when $V0$ is also large (e.g., $V0 = 1$). This is particularly true for the kappa-Maxwellian plasma. The linear analysis still remains valid as $(\text{Im}W)_{\text{max}} / (\text{Re}W)_{\text{max}} \leq 0.2$ under those conditions. All it suggests is a faster onset of the nonlinear processes. However, according to Fig. 1, the instability can be excited with a much smaller $V0 (\ll 1)$ when $T_{e\parallel} / T_{i\parallel} > 1$ and $T_{i\parallel} / T_{i\perp} > 1$. For example, (1) when $T_{e\parallel} / T_{i\parallel} = 1$ and $T_{i\parallel} / T_{i\perp} = 5$, $V_{C,M} \cong 0.28$ and $V_{C,K} \cong 0.32$; (2) when $T_{e\parallel} / T_{i\parallel} = 5$ and $T_{i\parallel} / T_{i\perp} = 1$, $V_{C,M} \cong 0.14$ and $V_{C,K} \cong 0.17$; and (3) when $T_{e\parallel} / T_{i\parallel} = 5$ and $T_{i\parallel} / T_{i\perp} = 5$, $V_{C,M} \cong 0.12$ and $V_{C,K} \cong 0.14$. Here, $V_{C,M(K)}$ refers to the threshold value V_C for bi-Maxwellian (kappa-Maxwellian) plasma. The maximum linear growth rates of the instability are quite small when $V0$ is above and near these small threshold values (see Fig. 2) and,

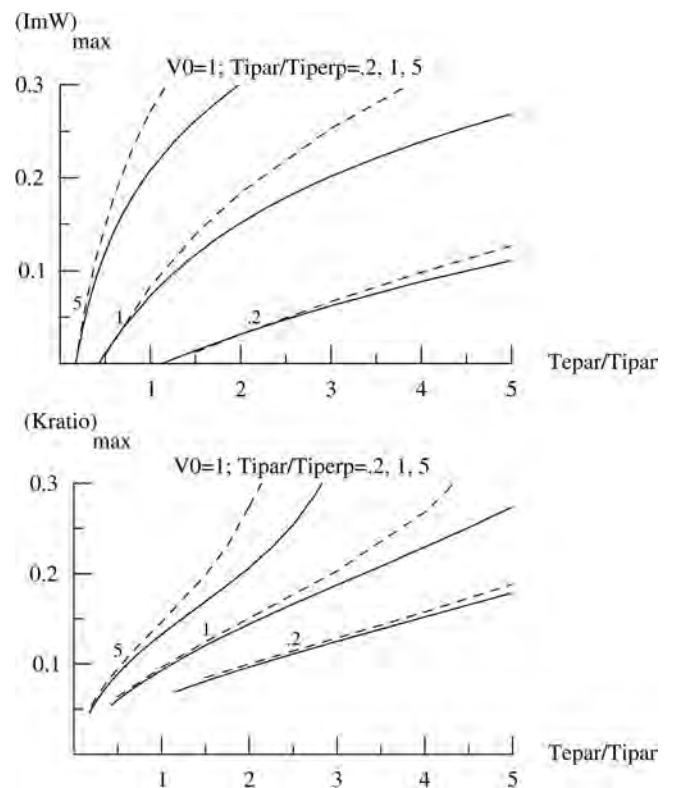


FIG. 4. (Top panel) $\text{Im}W (\equiv \text{Im} \omega / \Omega_i)$, maximized with respect to k_{\parallel} and k_{\perp} , and (bottom panel) $(k_{\parallel} / k_{\perp})$, for which the maximum values of $\text{Im}W$ are obtained, as a function of $T_{e\parallel} / T_{i\parallel}$ for $\omega_{pe} / \Omega_e = 1/15$, $V0 (\equiv V_0 / V_{e\parallel}) = 1$, and selected values of $T_{i\parallel} / T_{i\perp}$. The solid curves represent results for bi-Maxwellian plasma and the dashed curves represent results for kappa-Maxwellian ($\kappa_e = \kappa_i = 3$) plasma. The curves are labeled by the selected values of $T_{i\parallel} / T_{i\perp}$.

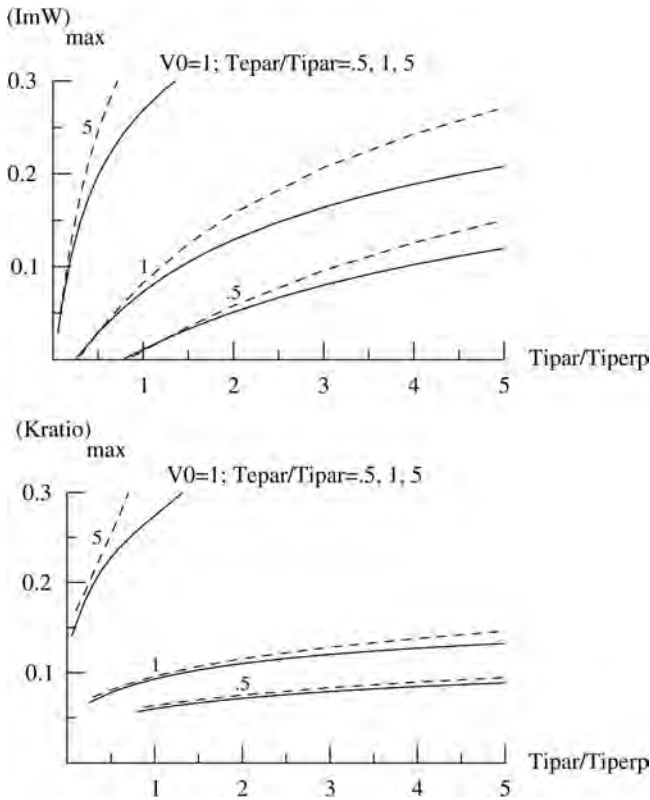


FIG. 5. (Top panel) $\text{Im}W(\equiv \text{Im}\omega/\Omega_i)$, maximized with respect to k_{\parallel} and k_{\perp} , and (bottom panel) $(k_{\parallel}/k_{\perp})$, for which the maximum values of $\text{Im}W$ are obtained, as a function of $T_{e\parallel}/T_{i\perp}$ for $\omega_{pe}/\Omega_e = 1/15$, $V_0(\equiv V_0/V_{e\parallel}) = 1$, and selected values of $T_{e\parallel}/T_{i\parallel}$. The solid curves represent results for bi-Maxwellian plasma and the dashed curves represent results for kappa-Maxwellian ($\kappa_e = \kappa_i = 3$) plasma. The curves are labeled by the selected values of $T_{e\parallel}/T_{i\parallel}$.

for such values of V_0 , the linear stability analysis is certainly appropriate. In the following presentation of the various characteristics of the unstable ion-cyclotron modes in the two types of plasma, we have used $V_0 = 1$ in order to cover a large range of values of $T_{e\parallel}/T_{i\parallel}$ and $T_{i\parallel}/T_{i\perp}$ for which the instability occurs (see Fig. 1).

The top panel of Fig. 4 shows $(\text{Im}W)_{\text{max}}$, defined as above, as a function of $T_{e\parallel}/T_{i\parallel}$ for selected values of $T_{i\parallel}/T_{i\perp}$. It is evident that, for a fixed $T_{i\parallel}/T_{i\perp}$, $(\text{Im}W)_{\text{max}}$ increases with $T_{e\parallel}/T_{i\parallel}$ (rate of increase being larger for a larger $T_{i\parallel}/T_{i\perp}$) and that it increases more rapidly in kappa-Maxwellian plasma. The bottom panel shows the values of k_{\parallel}/k_{\perp} [denoted by $(\text{Kratio})_{\text{max}}$], for which $(\text{Im}W)_{\text{max}}$ are obtained, as a function of $T_{e\parallel}/T_{i\parallel}$ for the same selected values of $T_{i\parallel}/T_{i\perp}$. It shows that the angle (between \mathbf{k} and \mathbf{B}_0) of propagation of the maximum unstable modes becomes smaller with increasing values of $T_{e\parallel}/T_{i\parallel}$ (i.e., the modes propagate more parallel to \mathbf{B}_0) and that this change in the angle of propagation occurs more rapidly in kappa-Maxwellian plasma. Figure 4 also indicates that, for a fixed $T_{e\parallel}/T_{i\parallel}$, both $(\text{Im}W)_{\text{max}}$ and $(\text{Kratio})_{\text{max}}$ increase substantially as $T_{i\parallel}/T_{i\perp}$ increases. These are shown more explicitly in the top and bottom panels of Fig. 5. Numerical analysis further shows that the magnitudes of $(\text{Im}W)_{\text{max}}$ and $(\text{Kratio})_{\text{max}}$ as a function of $T_{e\parallel}/T_{i\parallel}$ and $T_{i\parallel}/T_{i\perp}$ in both types of plasma depend on the choice of the value of $V_0 > V_C$.

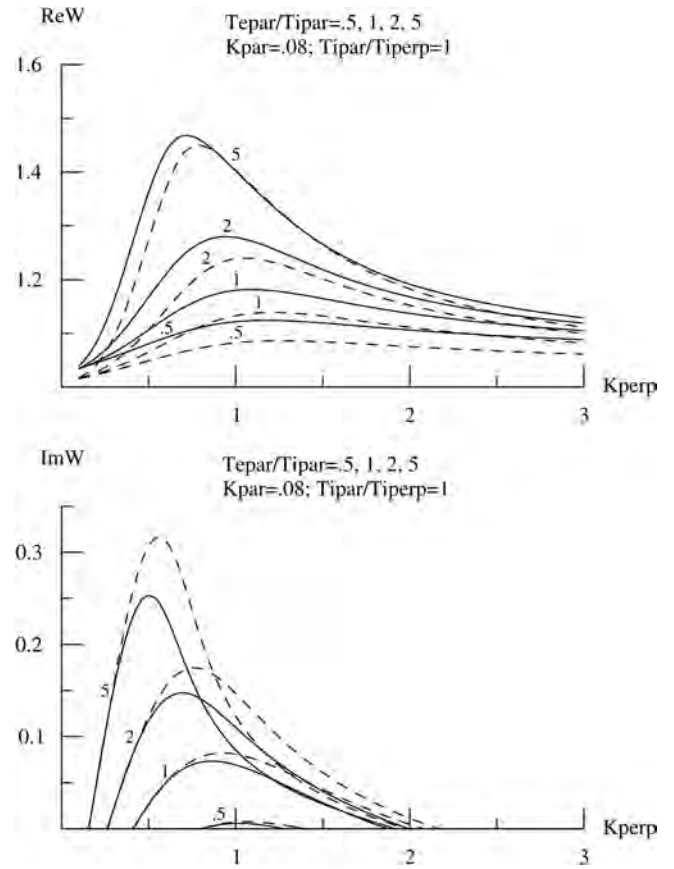


FIG. 6. (Top panel) $\text{Re}W(\equiv \text{Re}\omega/\Omega_i)$ vs. $K_{\perp}(\equiv K_{\text{perp}}) = k_{\perp}\rho_i$ and (bottom panel) $\text{Im}W(\equiv \text{Im}\omega/\Omega_i)$ vs. K_{\perp} for $\omega_{pe}/\Omega_e = 1/15$, $V_0(\equiv V_0/V_{e\parallel}) = 1$, $K_{\parallel}(\equiv K_{\text{par}}) = k_{\parallel}\rho_i = 0.08$, $T_{i\parallel}/T_{i\perp} = 1$, and selected values of $T_{e\parallel}/T_{i\parallel}$. The solid curves represent results for bi-Maxwellian plasma and the dashed curves represent results for kappa-Maxwellian ($\kappa_e = \kappa_i = 3$) plasma. The curves are labeled by the selected values of $T_{e\parallel}/T_{i\parallel}$.

Figures 6–9 show the spectral (ω vs \mathbf{k}) behavior of the unstable ion-cyclotron modes for the selected values of $T_{e\parallel}/T_{i\parallel}$ and $T_{i\parallel}/T_{i\perp}$. In these figures, $K_{\text{par}}(\equiv K_{\parallel}) = k_{\parallel}\rho_i$ and $K_{\text{perp}}(\equiv K_{\perp}) = k_{\perp}\rho_i$, where ρ_i is the ion gyroradius. Figures 6 and 7 show $\text{Re}W$ and $\text{Im}W$ versus $K_{\perp} = 0.08$ and various values of $T_{e\parallel}/T_{i\parallel}$ and $T_{i\parallel}/T_{i\perp}$. They show that, for a given $T_{i\parallel}/T_{i\perp}$ (or $T_{e\parallel}/T_{i\parallel}$), $\text{Re}\omega$ moves closer to Ω_i and the growth rate ($\text{Im}\omega$) decreases (suggesting larger critical drift) as $T_{e\parallel}/T_{i\parallel}$ (or $T_{i\parallel}/T_{i\perp}$) decreases. Conversely, $\text{Re}\omega$ moves away from Ω_i and the growth rate increases (suggesting smaller critical drift) as $T_{e\parallel}/T_{i\parallel}$ (or $T_{i\parallel}/T_{i\perp}$) increases. These conclusions hold for both bi-Maxwellian and kappa-Maxwellian plasmas. However, as the figures show, there are significant quantitative differences between the unstable spectra in the two types of plasma. Magnitudes of these differences depend on the values of $T_{e\parallel}/T_{i\parallel}$ and $T_{i\parallel}/T_{i\perp}$ for the assumed values of κ_e , κ_i , and V_0 . The real frequencies are smaller in kappa-Maxwellian plasma than in bi-Maxwellian plasma for all values of K_{\perp} . On the other hand, the growth rates are larger in kappa-Maxwellian plasma than in bi-Maxwellian plasma beyond some values of K_{\perp} . Additionally, the unstable spectra in kappa-Maxwellian plasma extend to comparatively larger values of K_{\perp} . Figures 8 and 9 show $\text{Re}W$ and $\text{Im}W$ versus K_{\parallel} , for $K_{\perp} = 0.8$ and values of

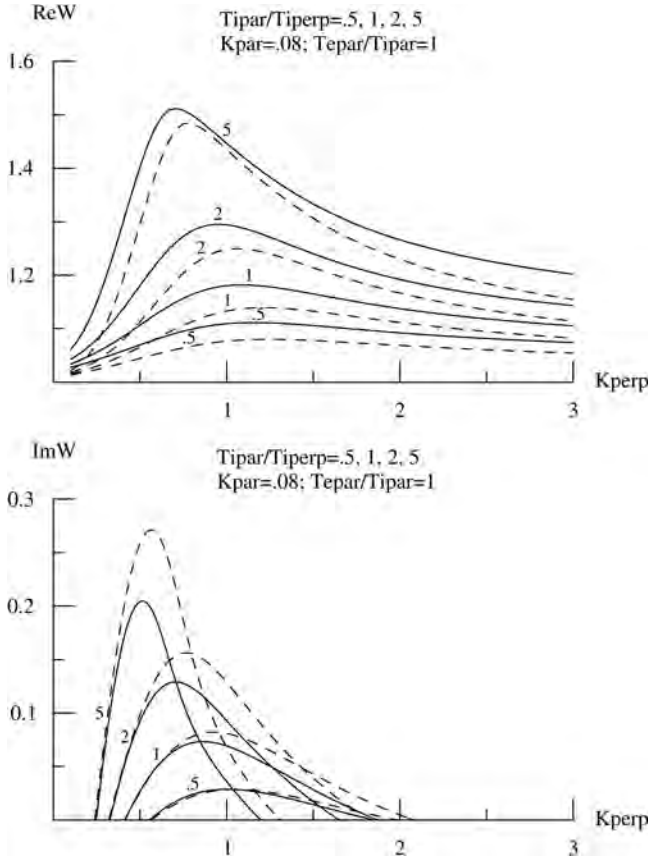


FIG. 7. (Top panel) $\text{Re}W(\equiv \text{Re}\omega/\Omega_i)$ vs. $K_{\perp}(\equiv K_{\text{perp}}) = k_{\perp}\rho_i$ and (bottom panel) $\text{Im}W(\equiv \text{Im}\omega/\Omega_i)$ vs. K_{\perp} for $\omega_{pe}/\Omega_e = 1/15$, $V_0(\equiv V_0/V_{e\parallel}) = 1$, $K_{\parallel}(\equiv K_{\text{par}}) = k_{\parallel}\rho_i = 0.08$, $T_{e\parallel}/T_{i\parallel} = 1$, and selected values of $T_{e\parallel}/T_{i\perp}$. The solid curves represent results for bi-Maxwellian plasma and the dashed curves represent results for kappa-Maxwellian ($\kappa_e = \kappa_i = 3$) plasma. The curves are labeled by the selected values of $T_{e\parallel}/T_{i\perp}$.

$T_{e\parallel}/T_{i\parallel}$ and $T_{e\parallel}/T_{i\perp}$ same as those in Figs. 6 and 7. They show similar (to Figs. 6 and 7) functional dependence of the unstable spectra on $T_{e\parallel}/T_{i\parallel}$, $T_{e\parallel}/T_{i\perp}$, and similar differences between the unstable spectra in the two types of plasma as a function of K_{\parallel} . Both the K_{\perp} - and the K_{\parallel} -dependence of $\text{Im}W$ and their differences in the two types of plasmas may be understood in terms of the combined effects of the electron drive (Landau growth) and the ion cyclotron damping.

For heavier-ion plasma, qualitatively similar, but quantitatively different due to increased ion mass, results are obtained. We do not present those results here. Instead, more interesting effects of the parameter ω_{pe}/Ω_e on the stability properties of the ion-cyclotron modes are presented next. Figure 10 shows the variation of V_C (threshold value of V_0 normalized to $V_{e\parallel}$) with respect to $\omega_{pe}/\Omega_e \equiv \sigma$ (Sigma) for $T_{e\parallel}/T_{i\parallel} = 1$ and different values of $T_{e\parallel}/T_{i\perp}$. When σ is less than 0.02, V_C is large exceeding unity. As σ increases, V_C decreases sharply and then settles down to a value, which is nearly independent of σ . Furthermore, the values of V_C are larger for smaller values of $T_{e\parallel}/T_{i\perp}$ and for all values of σ . The same functional behavior is found for both types of plasma. However, as evident from the figure, there are appreciable quantitative differences between the two types of plasma. The top and bottom panels of Fig. 11, which are

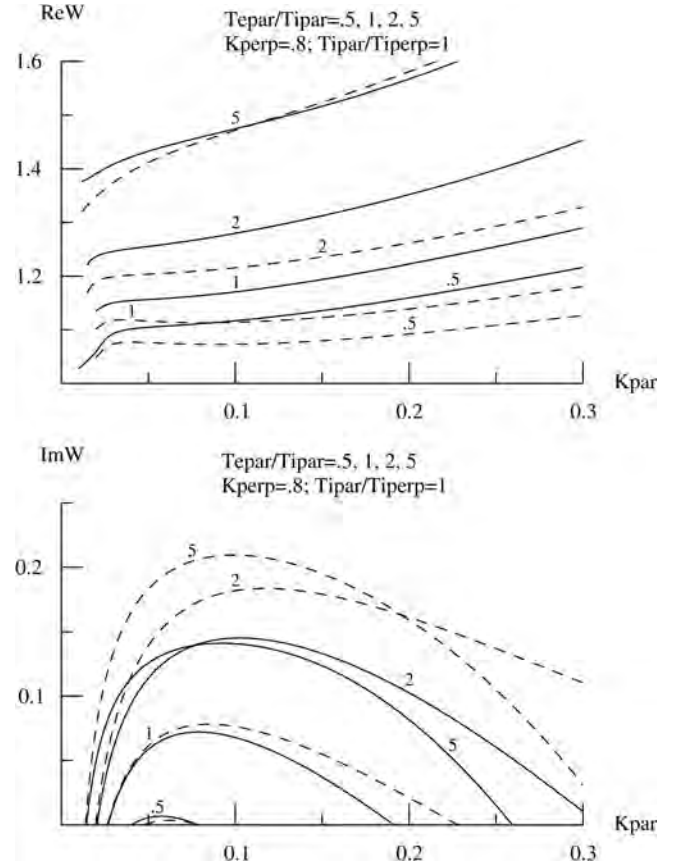


FIG. 8. (Top panel) $\text{Re}W(\equiv \text{Re}\omega/\Omega_i)$ vs. $K_{\parallel}(\equiv K_{\text{par}}) = k_{\parallel}\rho_i$ and (bottom panel) $\text{Im}W(\equiv \text{Im}\omega/\Omega_i)$ vs. K_{\parallel} for $\omega_{pe}/\Omega_e = 1/15$, $V_0(\equiv V_0/V_{e\parallel}) = 1$, $K_{\perp}(\equiv K_{\text{perp}}) = k_{\perp}\rho_i = 0.8$, $T_{i\parallel}/T_{i\perp} = 1$, and selected values of $T_{e\parallel}/T_{i\parallel}$. The solid curves represent results for bi-Maxwellian plasma and the dashed curves represent results for kappa-Maxwellian ($\kappa_e = \kappa_i = 3$) plasma. The curves are labeled by the selected values of $T_{e\parallel}/T_{i\parallel}$.

obtained for $V_0 = 1$, $T_{e\parallel}/T_{i\parallel} = 1$, and selected values of $T_{e\parallel}/T_{i\perp}$, show that $(\text{Im}W)_{\text{max}}$ and $(\text{Re}W)_{\text{max}}$, defined as above, decrease as σ decreases. The rate of decrement increases as $T_{e\parallel}/T_{i\perp}$ increases, and the instability disappears when σ is smaller than a certain value that depends on $T_{e\parallel}/T_{i\perp}$. The disappearance of the instability has to do with the fact that the electron drive decreases while the ion damping increases as σ decreases. Finally, Fig. 12 shows the dependence of $(\text{Kratio})_{\text{max}}$, defined as above, on σ for $V_0 = 1$, $T_{e\parallel}/T_{i\parallel} = 1$, and selected values of $T_{e\parallel}/T_{i\perp}$. For both types of plasma, the angle (between \mathbf{k} and \mathbf{B}_0) of propagation of the maximum unstable mode decreases, i.e., the mode propagates more parallel to \mathbf{B}_0 , with increasing σ . Quantitative differences between the two types of plasma are evident from the figures. Similar dependences on σ are found for other values of $T_{e\parallel}/T_{i\parallel}$, but they are not shown here. We have chosen $\sigma = 1/15$ in the presentation for illustration purposes only as V_C tends to be insensitive to σ around this value.

V. QUASILINEAR ION HEATING RATES

It has been argued that quasilinear plateau formation cannot stabilize the current-driven ion-cyclotron instability because of the slowly convecting nature of the modes and growth continues until other nonlinear mechanisms provide

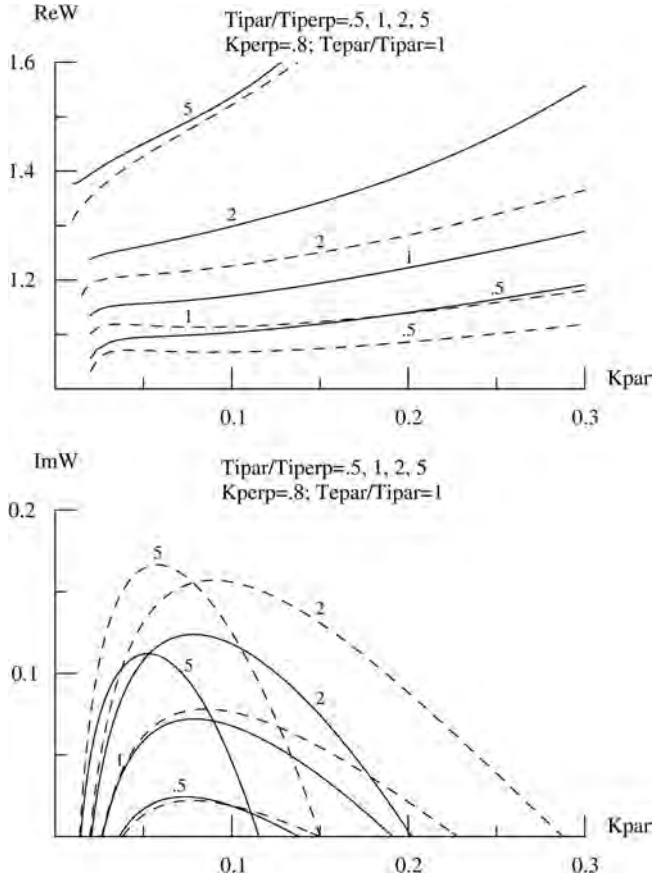


FIG. 9. (Top panel) $\text{Re}W(\equiv \text{Re}\omega/\Omega_i)$ vs. $K_{\parallel}(\equiv K_{\text{par}}) = k_{\parallel}\rho_i$ and (bottom panel) $\text{Im}W(\equiv \text{Im}\omega/\Omega_i)$ vs. K_{\parallel} for $\omega_{pe}/\Omega_e = 1/15$, $V_0(\equiv V_0/V_{e\parallel}) = 1$, $K_{\perp}(\equiv K_{\text{perp}}) = k_{\perp}\rho_i = 0.8$, $T_{e\parallel}/T_{i\perp} = 1$, and selected values of $T_{i\parallel}/T_{i\perp}$. The solid curves represent results for bi-Maxwellian plasma and the dashed curves represent results for kappa-Maxwellian ($\kappa_e = \kappa_i = 3$) plasma. The curves are labeled by the selected values of $T_{i\parallel}/T_{i\perp}$.

saturation.^{22,23,33} Quasilinear analysis, therefore, does not yield correct estimates of the ion heating rates. Nevertheless, for the purposes of comparison, we present here the quasilinear estimates of the ion heating rates due to ion-cyclotron turbulence in bi-Maxwellian and kappa-Maxwellian plasmas.

The quasilinear response of the magnetized ions to unstable electrostatic field fluctuations is described by³⁴

$$\begin{aligned} \frac{\partial}{\partial t} F_i(v_{\perp}^2, v_{\parallel}, t) = & i \frac{e^2}{m_i^2} \sum_{n=-\infty}^{+\infty} \int d\mathbf{k} |\tilde{\phi}(\mathbf{k}, t)|^2 \\ & \times \left(k_{\parallel} \frac{\partial}{\partial v_{\parallel}} + \frac{n\Omega_i}{v_{\perp}} \frac{\partial}{\partial v_{\perp}} \right) \frac{J_n^2(\mu)}{\omega_{\mathbf{k}} - k_{\parallel}v_{\parallel} - n\Omega_i} \\ & \times \left(k_{\parallel} \frac{\partial}{\partial v_{\parallel}} + \frac{n\Omega_i}{v_{\perp}} \frac{\partial}{\partial v_{\perp}} \right) F_i(v_{\perp}^2, v_{\parallel}, t), \end{aligned} \quad (26)$$

for small $\text{Im}\omega_{\mathbf{k}} \geq 0$. Here $\mu = k_{\perp}v_{\perp}/\Omega_i$, $\omega_{\mathbf{k}} = \omega(k_{\perp}, k_{\parallel})$ is the complex solution of the linear dispersion relation, and $\tilde{\phi}(\mathbf{k}, t)$ is the potential fluctuation, which, within the framework of the quasilinear theory, evolves adiabatically in time according to

$$\frac{\partial}{\partial t} |\tilde{\phi}(\mathbf{k}, t)|^2 = 2 \text{Im} \omega_{\mathbf{k}}(t) |\tilde{\phi}(\mathbf{k}, t)|^2. \quad (27)$$

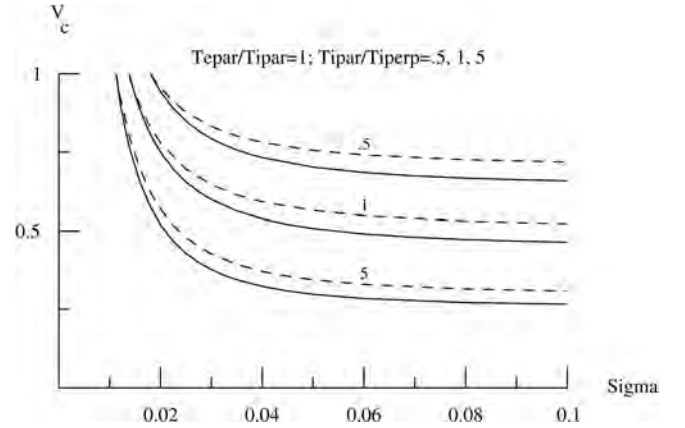


FIG. 10. Threshold (critical) value of electron drift speed, normalized to $V_{e\parallel}$ and denoted by V_c , as a function of $\omega_{pe}/\Omega_e = \sigma$ (Sigma) for $T_{e\parallel}/T_{i\parallel} = 1$ and selected values of $T_{i\parallel}/T_{i\perp}$. The solid curves represent results for bi-Maxwellian plasma and the dashed curves represent results for kappa-Maxwellian ($\kappa_e = \kappa_i = 3$) plasma. The curves are labeled by the selected values of $T_{i\parallel}/T_{i\perp}$.

We assume that the fundamental harmonic is the dominant mode and so keep $n = 1$ term only. Then, in the resonant region of velocity space ($\text{Re}\omega_{\mathbf{k}} - k_{\parallel}v_{\parallel} - \Omega_i = 0$), Eq. (26) can be approximated by³⁴

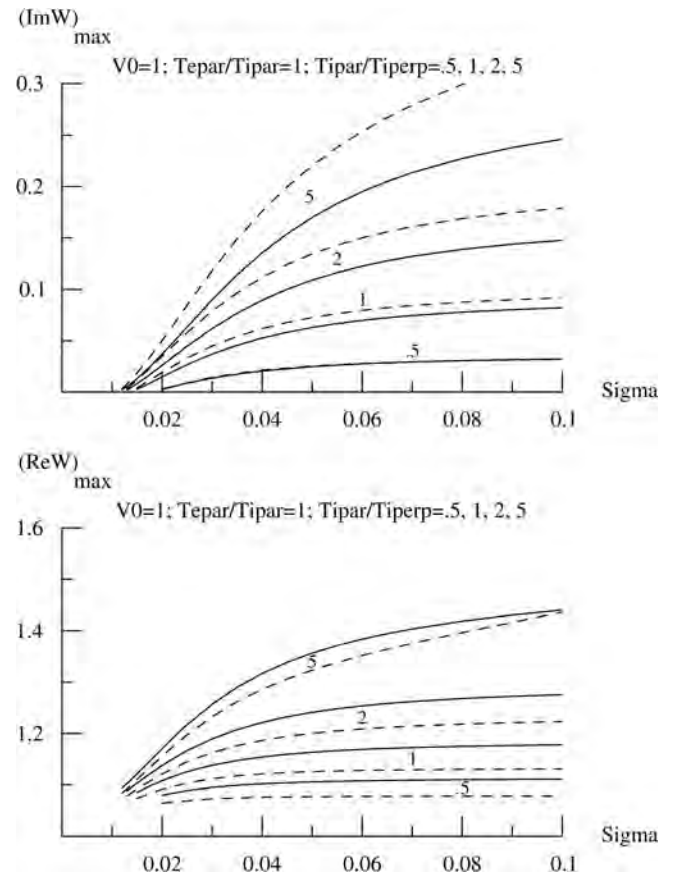


FIG. 11. (Top panel) $\text{Im}W(\equiv \text{Im}\omega/\Omega_i)$, maximized with respect to k_{\parallel} and k_{\perp} and (bottom panel) $\text{Re}W(\equiv \text{Re}\omega/\Omega_i)$, corresponding to the $(\text{Im}W)_{\text{max}}$, as a function of $\omega_{pe}/\Omega_e = \sigma$ (Sigma) for $V_0(\equiv V_0/V_{e\parallel}) = 1$, $T_{e\parallel}/T_{i\parallel} = 1$, and selected values of $T_{i\parallel}/T_{i\perp}$. The solid curves represent results for bi-Maxwellian plasma and the dashed curves represent results for kappa-Maxwellian ($\kappa_e = \kappa_i = 3$) plasma. The curves are labeled by the selected values of $T_{i\parallel}/T_{i\perp}$.

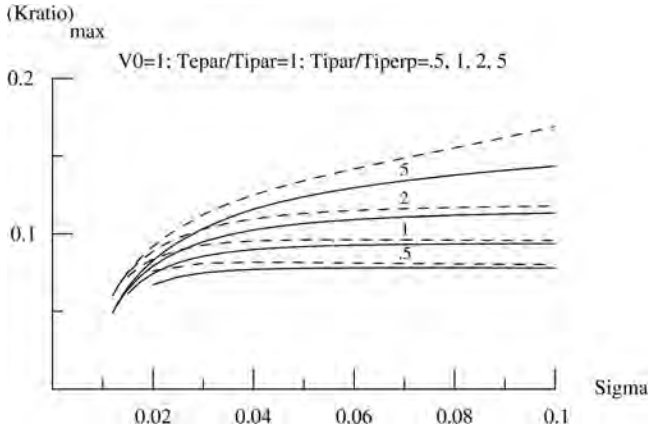


FIG. 12. Values of $(k_{\parallel}/k_{\perp})$, for which the maximum values of $\text{Im}W$ shown in Fig. 11 are obtained, as a function of $\omega_{pe}/\Omega_e = \sigma$ (Sigma) for $V_0(\equiv V_0/V_{e\parallel}) = 1$, $T_{e\parallel}/T_{i\parallel} = 1$, and selected values of $T_{i\parallel}/T_{i\perp}$. The solid curves represent results for bi-Maxwellian plasma and the dashed curves represent results for kappa-Maxwellian ($\kappa_e = \kappa_i = 3$) plasma. The curves are labeled by the selected values of $T_{i\parallel}/T_{i\perp}$.

$$\begin{aligned} \frac{\partial}{\partial t} F_i(v_{\perp}^2, v_{\parallel}, t) = & \frac{\pi e^2}{m_i^2} \int d\mathbf{k} |\tilde{\phi}(\mathbf{k}, t)|^2 \left(k_{\parallel} \frac{\partial}{\partial v_{\parallel}} + \frac{\Omega_i}{v_{\perp}} \frac{\partial}{\partial v_{\perp}} \right) J_1^2(\mu) \\ & \times \delta(\text{Re} \omega_{\mathbf{k}} - k_{\parallel} v_{\parallel} - \Omega_i) \left(k_{\parallel} \frac{\partial}{\partial v_{\parallel}} + \frac{\Omega_i}{v_{\perp}} \frac{\partial}{\partial v_{\perp}} \right) \\ & \times F_i(v_{\perp}^2, v_{\parallel}, t), \end{aligned} \quad (28)$$

under the small $\text{Im} \omega_{\mathbf{k}}$ assumption. Here, $\delta(x)$ is the Dirac δ function. Multiplying Eq. (28) by $m_i v_{\perp}^2/2$, using Eqs. (2) and (7) for F_i on the right-hand side (for estimation purposes), and integrating over velocities, we find

$$\frac{d}{dt} T_{i\perp} = \sqrt{\frac{\pi m_i}{2T_{i\parallel}}} \frac{e^2 \Omega_i^2}{T_{i\parallel}} \int \frac{d\mathbf{k}}{|k_{\parallel}|} |\tilde{\phi}(\mathbf{k}, t)|^2 \Lambda_1(b_i) I(k_{\perp}, k_{\parallel}), \quad (29)$$

where

$$I(k_{\perp}, k_{\parallel}) = \left(\frac{\text{Re} \omega_{\mathbf{k}} - \Omega_i}{\Omega_i} + \frac{T_{i\parallel}}{T_{i\perp}} \right) \exp(-\eta_{i\mathbf{k}}^2) \equiv I_{\text{BM}}, \quad (30)$$

for bi-Maxwellian plasma, and

$$\begin{aligned} I(k_{\perp}, k_{\parallel}) = & f(\kappa_i) \left(\frac{2\kappa_i}{2\kappa_i - 1} \right)^{3/2} \left(1 + \frac{\eta_{i\mathbf{k}}^2}{\kappa_i - 1/2} \right)^{-(\kappa_i + 1)} \\ & \times \left[\left(1 + \frac{\eta_{i\mathbf{k}}^2}{\kappa_i - 1/2} \right)^{-1} \frac{\kappa_i + 1}{\kappa_i} \frac{\text{Re} \omega_{\mathbf{k}} - \Omega_i}{\Omega_i} \right. \\ & \left. + \frac{2\kappa_i - 1}{2\kappa_i} \frac{T_{i\parallel}}{T_{i\perp}} \right] \equiv I_{\text{KM}}, \end{aligned} \quad (31)$$

for kappa-Maxwellian plasma, provided $\kappa_i > 1/2$. Here $\eta_{i\mathbf{k}} \equiv (\text{Re} \omega_{\mathbf{k}} - \Omega_i)/(\sqrt{2}k_{\parallel}V_{i\parallel})$. Figure 13 shows $I(k_{\perp}, k_{\parallel})$ as a function of the unstable values of $K_{\parallel}(\equiv k_{\parallel}\rho_i)$, for $K_{\perp}(\equiv k_{\perp}\rho_i) = 0.8$, $\omega_{pe}/\Omega_e = 1/15$, $V_0(\equiv V_0/V_{e\parallel}) = 1$, $T_{e\parallel}/T_{i\parallel} = 1$, and selected values of $T_{i\parallel}/T_{i\perp}$. The solid curves represent I_{BM} given by Eq. (30) for bi-Maxwellian plasma and the dashed curves represent I_{KM} given by Eq. (31) for kappa-Maxwellian plasma. The figure shows that $I_{\text{KM}} > I_{\text{BM}}$

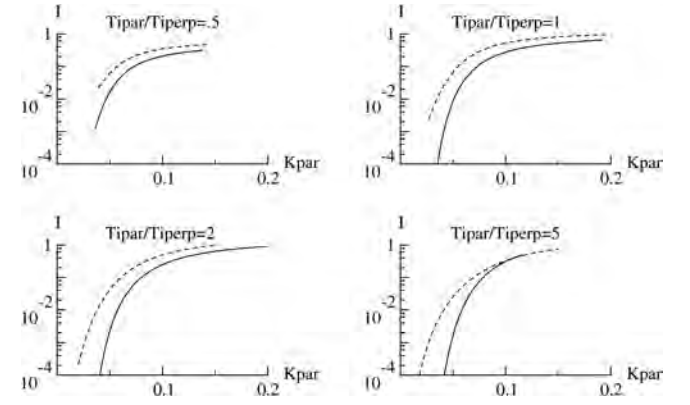


FIG. 13. The function I appearing in Eq. (29) vs. unstable values of $K_{\parallel}(\equiv k_{\parallel}\rho_i)$ for $K_{\perp}(\equiv k_{\perp}\rho_i) = 0.8$, $\omega_{pe}/\Omega_e = 1/15$, $V_0(\equiv V_0/V_{e\parallel}) = 1$, $T_{e\parallel}/T_{i\parallel} = 1$, and selected values of $T_{i\parallel}/T_{i\perp}$. The solid curves represent I given by Eq. (30) for bi-Maxwellian plasma and the dashed curves represent I given by Eq. (31) for kappa-Maxwellian ($\kappa_e = \kappa_i = 3$) plasma.

over almost the entire unstable K_{\parallel} spectrum. This is basically due to the power-law dependence of I_{KM} on $\eta_{i\mathbf{k}}$, in contrast with the exponential dependence of I_{BM} on $\eta_{i\mathbf{k}}$, when $|\eta_{i\mathbf{k}}| > 1$. Similar results are found for other values of $T_{e\parallel}/T_{i\parallel}$.

Next, multiplying Eq. (28) by $m_i v_{\parallel}^2$, using Eqs. (2) and (7) for F_i on the right-hand side (for estimation purpose), and integrating over velocities, we find

$$\frac{d}{dt} T_{i\parallel} = \sqrt{\frac{2\pi m_i}{T_{i\parallel}}} \frac{e^2 \Omega_i^2}{T_{i\parallel}} \int \frac{d\mathbf{k}}{|k_{\parallel}|} |\tilde{\phi}(\mathbf{k}, t)|^2 \Lambda_1(b_i) J(k_{\perp}, k_{\parallel}), \quad (32)$$

where

$$J(k_{\perp}, k_{\parallel}) = (\text{Re} \omega_{\mathbf{k}}/\Omega_i - 1) I_{\text{BM}} \equiv J_{\text{BM}}, \quad (33)$$

for bi-Maxwellian plasma, and

$$J(k_{\perp}, k_{\parallel}) = (\text{Re} \omega_{\mathbf{k}}/\Omega_i - 1) I_{\text{KM}} \equiv J_{\text{KM}}, \quad (34)$$

for kappa-Maxwellian plasma. Figure 14 shows $J(k_{\perp}, k_{\parallel})$ as a function of the unstable values of $K_{\parallel}(\equiv k_{\parallel}\rho_i)$, for $K_{\perp}(\equiv k_{\perp}\rho_i) = 0.8$, $\omega_{pe}/\Omega_e = 1/15$, $V_0(\equiv V_0/V_{e\parallel}) = 1$, $T_{e\parallel}/T_{i\parallel} = 1$, and selected values of $T_{i\parallel}/T_{i\perp}$. The solid curves represent J_{BM} given by Eq. (33) for bi-Maxwellian plasma and the dashed curves represent J_{KM} given by Eq. (34) for kappa-Maxwellian plasma. The figure shows that $J_{\text{KM}} > J_{\text{BM}}$ over almost the entire unstable K_{\parallel} spectrum. Once again, this is basically due to the power-law dependence of J_{KM} on $\eta_{i\mathbf{k}}$, in contrast with the exponential dependence of J_{BM} on $\eta_{i\mathbf{k}}$, when $|\eta_{i\mathbf{k}}| > 1$. Similar results are found for other values of $T_{e\parallel}/T_{i\parallel}$.

Furthermore, we may estimate that

$$\frac{dT_{i\perp}/dt}{dT_{i\parallel}/dt} \approx \frac{I_{\text{BM}}}{2J_{\text{BM}}} \equiv \frac{1}{2} \frac{\Omega_i}{\text{Re} \omega_{\mathbf{k}} - \Omega_i}, \quad (35)$$

for bi-Maxwellian plasma and

$$\frac{dT_{i\perp}/dt}{dT_{i\parallel}/dt} \approx \frac{I_{\text{KM}}}{2J_{\text{KM}}} \equiv \frac{1}{2} \frac{\Omega_i}{\text{Re} \omega_{\mathbf{k}} - \Omega_i}, \quad (36)$$

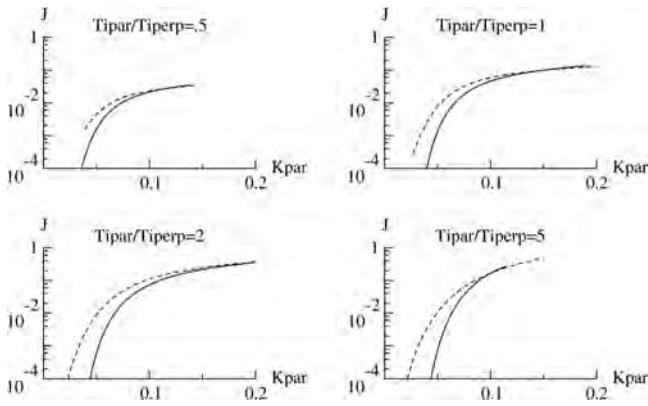


FIG. 14. The function J appearing in Eq. (32) vs. unstable values of $K_{\parallel} (\equiv k_{\parallel} \rho_i)$ for $K_{\perp} (\equiv k_{\perp} \rho_i) = 0.8$, $\omega_{pe}/\Omega_e = 1/15$, $V_0 (\equiv V_0/V_{e\parallel}) = 1$, $T_{e\parallel}/T_{i\parallel} = 1$, and selected values of $T_{i\parallel}/T_{i\perp}$. The solid curves represent J given by Eq. (33) for bi-Maxwellian plasma and the dashed curves represent J given by Eq. (34) for kappa-Maxwellian ($\kappa_e = \kappa_i = 3$) plasma.

for kappa-Maxwellian plasma. Although the right-hand side of Eqs. (35) and (36) is formally the same, they are quite different for bi-Maxwellian and kappa-Maxwellian plasmas. In fact, numerical solutions of the linear dispersion relations show that $(\text{Re } \omega_k - \Omega_i)/\Omega_i \ll 1$ for both types of plasma, but $(\text{Re } \omega_k - \Omega_i)/\Omega_i$ has smaller values for kappa-Maxwellian plasma, when V_0 , $T_{e\parallel}/T_{i\parallel}$, and $T_{i\parallel}/T_{i\perp}$ are not too large [see Figs. 6–9]. Equations (35) and (36) then suggest that, under these conditions, ions are heated preferentially in the perpendicular direction and this effect is enhanced in kappa-Maxwellian plasma. These conclusions can also be derived from Figs. 13 and 14 where I_{BM} , I_{KM} , J_{BM} , and J_{KM} are shown.

VI. SUMMARY

We have presented for the first time the linear stability properties of the current-driven electrostatic ion-cyclotron modes in kappa-Maxwellian plasma where the parallel velocity distributions of electrons and protons are modeled by kappa distributions and the perpendicular velocity distributions are modeled by Maxwellian distributions with parallel temperatures different from perpendicular temperatures. In particular, dependence of the stability properties on various parameters, such as V_0 , k_{\parallel} , k_{\perp} , $T_{e\parallel}/T_{i\parallel}$, $T_{i\parallel}/T_{i\perp}$, and ω_{pe}/Ω_e , has been discussed in some details. For comparison, we have also presented the corresponding results for bi-Maxwellian plasma where both the parallel and the perpendicular velocity distributions are modeled by Maxwellian distributions with parallel temperatures different from perpendicular temperatures. Quasilinear estimates of resonant ion heating rates due to ion-cyclotron turbulence in the two types of plasma have also been presented for comparison. In order to gain some preliminary understanding of the linear instability in kappa-Maxwellian plasma and its comparison with that in bi-Maxwellian plasma, we have included approximate analytical solutions of the dispersion relations. But, more emphasis has been given on the numerical solutions of the dispersion relations in order to provide accurate and comprehensive comparison over a wide range of values of the various plasma parameters. Numerical analysis has been carried

out for electron-proton plasma. Qualitatively similar, but quantitatively different due to increased ion mass, results are expected for heavier-ion plasma.

Linear stability properties of the current-driven electrostatic ion cyclotron modes, as well as the quasilinear ion heating rates due to ion-cyclotron turbulence, in bi-Maxwellian and kappa-Maxwellian plasmas are qualitatively similar. However, there are quantitative differences, which can be significant, depending on the values of κ_e and κ_i . The important conclusions of the comparative study are summarized as follows.

- (1) The threshold (critical) value of the electron drift speed (i.e., current), above which the current-driven ion-cyclotron instability is excited, is larger in kappa-Maxwellian plasma for all values of $T_{i\parallel}/T_{i\perp}$ and for all $T_{e\parallel}/T_{i\parallel}$ above certain value, which increases with decreasing $T_{i\parallel}/T_{i\perp}$ (see Fig. 1).
- (2) Above and near the threshold (critical) value of the electron drift speed, the maximum growth rates are smaller in kappa-Maxwellian plasma. But, as V_0 is increased, the maximum growth rates become larger in kappa-Maxwellian plasma. Additionally, the unstable spectra in kappa-Maxwellian plasma extend to comparatively larger values of $K_{\perp} (\equiv k_{\perp} \rho_i)$ and $K_{\parallel} (\equiv k_{\parallel} \rho_i)$ (see Figs. 2, 6–9). The frequencies of the unstable modes are smaller in kappa-Maxwellian plasma (see Figs. 3, 6–9). These conclusions are valid for all values of $T_{e\parallel}/T_{i\parallel}$ and $T_{i\parallel}/T_{i\perp}$ for which the instability can be excited with a given V_0 .
- (3) The angle (between \mathbf{k} and \mathbf{B}_0) of propagation of the maximum unstable mode decreases with increasing $T_{e\parallel}/T_{i\parallel}$ and $T_{i\parallel}/T_{i\perp}$ in both bi-Maxwellian and kappa-Maxwellian plasmas. In other words, as $T_{e\parallel}/T_{i\parallel}$ and $T_{i\parallel}/T_{i\perp}$ increase, the maximum unstable mode propagates more parallel to \mathbf{B}_0 . However, the change in the angle of propagation occurs more rapidly in kappa-Maxwellian plasma (see bottom panels of Figs. 4 and 5). The magnitude of the change in the angle of propagation as well as the magnitude of the differences between the bi-Maxwellian and kappa-Maxwellian plasmas depends on the value of $V_0 > V_C$.
- (4) The threshold (critical) value of the electron drift speed, above which the current-driven ion-cyclotron instability is excited, decreases sharply as ω_{pe}/Ω_e increases and then settles down to a value, which is nearly independent of ω_{pe}/Ω_e , for both bi-Maxwellian and kappa-Maxwellian plasmas (see Fig. 10). For both types of plasma, the maximum value of $\text{Im } W (\equiv \text{Im } \omega/\Omega_i)$ and the corresponding value of $\text{Re } W (\equiv \text{Re } \omega/\Omega_i)$ decrease as ω_{pe}/Ω_e decreases. The rate of decrement increases as $T_{i\parallel}/T_{i\perp}$ increases, and the instability disappears when ω_{pe}/Ω_e is smaller than a certain value, which depends on $T_{i\parallel}/T_{i\perp}$ (see Fig. 11). For both types of plasma, the angle (between \mathbf{k} and \mathbf{B}_0) of propagation of the maximum unstable mode decreases, i.e., the mode propagates more parallel to \mathbf{B}_0 , with increasing ω_{pe}/Ω_e (see Fig. 12). Quantitative differences between the two types of plasma are evident from the figures.

(5) Quasilinear estimates of the resonant ion heating rates suggest that both the perpendicular and the parallel heating rates are larger in kappa-Maxwellian plasma. This is basically due to the power-law dependence (as opposed to the exponential dependence) on v_{\parallel} of the distribution of resonant ions in kappa-Maxwellian plasma [see Eqs. (29)–(34)]. They also suggest that, under certain conditions, ions are heated preferentially in the perpendicular direction in both bi-Maxwellian and kappa-Maxwellian plasmas, but this effect is enhanced in kappa-Maxwellian plasma.

The present study is based on nonrelativistic kappa distributions. For some space plasma, highly energetic particles are better modeled by relativistic kappa distributions. The reader is referred to the works by Xiao³⁵ and Xiao *et al.*^{36–38} for relativistic kappa distributions.

ACKNOWLEDGMENTS

This work was supported in part by the Air Force Office of Scientific Research (AFOSR).

- ¹V. Pierrard and M. Lazar, e-print arXiv:1003.3532v1 [physics.space-ph], 2010 and references therein.
²V. M. Vasyliunas, *J. Geophys. Res. [Space Phys.]* **73**, 2839, doi: 10.1029/JA073i009p02839 (1968).
³D. Summers and R. M. Thorne, *Phys. Fluids B* **3**, 1835 (1991).
⁴R. M. Thorne and D. Summers, *Phys. Fluids B* **3**, 2117 (1991).
⁵D. Summers and R. M. Thorne, *J. Geophys. Res. [Space Phys.]* **97**, 16827, doi: 10.1029/92JA01664 (1992).
⁶Z. Meng, R. M. Thorne, and D. Summers, *J. Plasma Phys.* **47**, 445 (1992).
⁷S. Xue, R. M. Thorne, and D. Summers, *J. Geophys. Res. [Space Phys.]* **98**, 17475, doi: 10.1029/93JA00790 (1993).
⁸D. Summers, S. Xue, and R. M. Thorne, *Phys. Plasmas* **1**, 2012 (1994).
⁹D. Summers and R. M. Thorne, *J. Plasma Phys.* **53**, 293 (1995).
¹⁰M. A. Hellberg and R. L. Mace, *Phys. Plasmas* **9**, 1495 (2002).
¹¹R. L. Mace and M. A. Hellberg, *Phys. Plasmas* **10**, 21 (2003).
¹²R. L. Mace, *Phys. Plasmas* **10**, 2181 (2003).

- ¹³R. L. Mace, *Phys. Plasmas* **11**, 507 (2004).
¹⁴R. P. Singhal and A. K. Tripathi, *Phys. Plasmas* **13**, 012102 (2006).
¹⁵F. Xiao, Q. Zhou, H. He, H. Zheng, and S. Wang, *J. Geophys. Res. [Space Phys.]* **112**, A07219, doi: 10.1029/2006JA012050 (2007).
¹⁶B. Basu, *Phys. Plasmas* **15**, 042108 (2008).
¹⁷B. Basu, *Phys. Plasmas* **16**, 052106 (2009).
¹⁸W. E. Drummond and M. N. Rosenbluth, *Phys. Fluids* **5**, 1507 (1962).
¹⁹J. M. Kindel and C. F. Kennel, *J. Geophys. Res. [Space Phys.]* **76**, 3055, doi: 10.1029/JA076i013p03055 (1971).
²⁰M. Ashour-Abdalla and R. M. Thorne, *J. Geophys. Res. [Space Phys.]* **83**, 4755, doi: 10.1029/JA083iA10p04755 (1978).
²¹K. F. Lee, *J. Plasma Phys.* **8**, 379 (1972).
²²H. Okuda and M. Ashour-Abdalla, *Geophys. Res. Lett.* **8**, 811, doi: 10.1029/GL008i007p00811 (1981).
²³H. Okuda and M. Ashour-Abdalla, *J. Geophys. Res. [Space Phys.]* **88**, 899, doi: 10.1029/JA088iA02p00899 (1983).
²⁴N. Singh, J. R. Conrad, and R. W. Schunk, *J. Geophys. Res. [Space Phys.]* **90**, 5159, doi: 10.1029/JA090iA06p05159 (1985).
²⁵H. Okuda and K. I. Nishikawa, *J. Geophys. Res. [Space Phys.]* **89**, 1023, doi: 10.1029/JA089iA02p01023 (1984).
²⁶G. S. Lakhina, *J. Geophys. Res. [Space Phys.]* **92**, 12161, doi: (1987).
²⁷N. Singh, J. R. Conrad, and R. W. Schunk, *J. Geophys. Res. [Space Phys.]* **90**, 12219, doi: 10.1029/JA090iA12p12219 (1985).
²⁸J. J. Rasmussen and R. W. Schrittwieser, *IEEE Trans. Plasma Sci.* **19**, 457 (1991).
²⁹N. A. Krall and A. W. Trivelpiece, *Principles of Plasma Physics* (McGraw-Hill, New York, 1973), p. 402.
³⁰B. D. Fried and S. D. Conte, *The Plasma Dispersion Function* (Academic, New York, 1961).
³¹R. L. Mace and M. A. Hellberg, *Phys. Plasmas* **2**, 2098 (1995).
³²D. Summers, R. M. Thorne, and H. Matsumoto, *Phys. Plasmas* **3**, 2496 (1996).
³³R. L. Lysak, M. K. Hudson, and M. Temerin, *J. Geophys. Res. [Space Phys.]* **85**, 678, doi: 10.1029/JA085iA02p00678 (1980).
³⁴R. C. Davidson, *Methods in Nonlinear Plasma Theory* (Academic, New York, 1972), pp. 160–166.
³⁵F. Xiao, *Plasma Phys. Controlled Fusion* **48**, 203 (2006).
³⁶F. Xiao, L. Chen, and J. Li, *Plasma Phys. Controlled Fusion* **50**, 1052002, doi: 10.1088/0741-3335/50/10/1052002 (2008).
³⁷F. Xiao, Q. Zhou, C. Li, and A. Cai, *Plasma Phys. Controlled Fusion* **50**, 062001, doi: 10.1088/0741-3335/50/6/062001 (2008).
³⁸F. Xiao, C. Shen, Y. Wang, H. Zheng, and S. Wang, *J. Geophys. Res. [Space Phys.]* **113**, A05203, doi: 10.1029/2007JA012903 (2008).

DISTRIBUTION LIST

DTIC/OCP 8725 John J. Kingman Rd, Suite 0944 Ft Belvoir, VA 22060-6218	1 cy
AFRL/RVIL Kirtland AFB, NM 87117-5776	2 cys
Official Record Copy AFRL/RVBXP/Daniel Ober	1 cy